

**Two perspectives on coupled exchange in the boundary layer**

M. Combe et al.

# Two perspectives on the coupled carbon, water, and energy exchange in the planetary boundary layer

M. Combe<sup>1</sup>, J. Vilà-Guerau de Arellano<sup>1</sup>, H. G. Ouwersloot<sup>2</sup>, C. M. J. Jacobs<sup>3</sup>, and W. Peters<sup>1,4</sup>

<sup>1</sup>Department of Meteorology and Air Quality, Wageningen University, Wageningen, the Netherlands

<sup>2</sup>Max Planck Institute for Chemistry, Mainz, Germany

<sup>3</sup>Climate change and Adaptive land and water management, Alterra Wageningen UR, Wageningen, the Netherlands

<sup>4</sup>Centre for Isotope Research, Groningen University, Groningen, the Netherlands

Received: 14 March 2014 – Accepted: 24 March 2014 – Published: 4 April 2014

Correspondence to: M. Combe (marie.combe@wur.nl)

Published by Copernicus Publications on behalf of the European Geosciences Union.

Title Page

Abstract

Introduction

Conclusions

References

Tables

Figures

◀

▶

◀

▶

Back

Close

Full Screen / Esc

Printer-friendly Version

Interactive Discussion



## Abstract

Understanding the interactions between the land surface and the atmosphere is key to model boundary-layer meteorology and cloud formation, as well as carbon cycling and crop yield. In this study we explore these interactions in the exchange of water, heat, and CO<sub>2</sub> in a cropland–atmosphere system at the diurnal and local scale. We thereto couple an atmospheric mixed-layer model (MXL) to two land-surface schemes, developed from two different perspectives: while one land-surface scheme (A-g<sub>s</sub>) simulates vegetation from an atmospheric point of view, the other (GECROS) simulates vegetation from a carbon-storage point of view. We calculate surface fluxes of heat, moisture and carbon, as well as the resulting atmospheric state and boundary-layer dynamics, over a maize field in the Netherlands, for a day on which we have a rich set of observations available. Particular emphasis is placed on understanding the role of upper atmosphere conditions like subsidence, in comparison to the role of surface forcings like soil moisture. We show that the atmospheric-oriented model (MXL-A-g<sub>s</sub>) outperforms the carbon storage-oriented model (MXL-GECROS) on this diurnal scale. This performance strongly depends on the sensitivity of the modelled stomatal conductance to water stress, which is implemented differently in each model. This sensitivity also influences the magnitude of the surface fluxes of CO<sub>2</sub>, water and heat (surface control), and subsequently impacts the boundary-layer growth and entrainment fluxes (upper atmosphere control), which alter the atmospheric state. These findings suggest that observed CO<sub>2</sub> mole fractions in the boundary layer can reflect strong influences of both the surface and upper atmospheric conditions, and the interpretation of CO<sub>2</sub> mole fraction variations depends on the assumed land-surface coupling. We illustrate this with a sensitivity analysis where increased subsidence, typical for periods of drought, can induce a change of 12 ppm in atmospheric CO<sub>2</sub> mole fractions, solely by decreasing the boundary-layer volume. The effect of such high subsidence on the Bowen ratio is of the same magnitude as induced by the depletion of soil moisture that would typically occur during a corresponding drought event. Correctly including such

BGD

11, 5275–5325, 2014

## Two perspectives on coupled exchange in the boundary layer

M. Combe et al.

Title Page

Abstract

Introduction

Conclusions

References

Tables

Figures



Back

Close

Full Screen / Esc

Printer-friendly Version

Interactive Discussion



two-way land-surface interactions on the diurnal scale can thus potentially improve our understanding and interpretation of observed variations in atmospheric CO<sub>2</sub>, as well as improve crop yield forecasts by better describing the water loss and carbon gain.

## 1 Introduction

5 The land surface and atmosphere interact on many time scales and understanding their exchange of energy, water, carbon, as well as chemical tracers, is key to many research fields including climate modelling (Cox et al., 2013; Sitch et al., 2008), crop yield prediction (Lobell et al., 2011), hydrology (Teuling et al., 2010), atmospheric composition (Bonan, 2008) and meteorology (Vilà-Guerau de Arellano et al., 2012). When  
10 the interaction concerns a vegetated surface and the planetary boundary layer overhead, the cycles of carbon, water, and energy are strongly coupled, notably at the surface. Responding to their environment, plants regulate the exchange of CO<sub>2</sub> and water vapor through the opening and closing of their stomata (Jarvis, 1976; Cowan, 1978; Ball, 1988), which in turn impacts the energy partitioning at the surface. This  
15 plant control over the carbon, water, and energy exchange plays a key role, especially in climate change studies, which is why the current generation of climate models all include mechanisms to describe the stomatal response of vegetation to changing environmental conditions (Farquhar et al., 1982; Collatz et al., 1991; Leuning et al., 1995; Jacobs et al., 1996). The ongoing rise of temperature and CO<sub>2</sub> concentration are already  
20 shown to affect the coupled cycles of water and carbon, as plants have become more efficient in water-use over the past decades (Keenan et al., 2013; Brien et al., 2011; Silva and Horwath, 2013). Quantitative understanding of these interactions between plants and the atmosphere is therefore needed.

25 The development of numerical models to describe land–atmosphere interactions is based on two perspectives. While vegetation models focus on carbon accumulation in land-surface types such as forests and crops and treat the atmosphere as a prescribed upper boundary condition, the atmospheric models focus on weather forecast and use

**BGD**

11, 5275–5325, 2014

## Two perspectives on coupled exchange in the boundary layer

M. Combe et al.

Title Page

Abstract

Introduction

Conclusions

References

Tables

Figures

◀

▶

◀

▶

Back

Close

Full Screen / Esc

Printer-friendly Version

Interactive Discussion



## Two perspectives on coupled exchange in the boundary layer

M. Combe et al.

Title Page

Abstract

Introduction

Conclusions

References

Tables

Figures



Back

Close

Full Screen / Esc

Printer-friendly Version

Interactive Discussion



the land surface as a prescribed lower boundary condition. The former group includes (dynamic) vegetation models and crop yield models such as LPJ (Sitch et al., 2003), ORCHIDEE-STICS (Smith et al., 2010), and CERES-maize (Bert et al., 2007). The latter includes submodels of numerical weather prediction systems and atmospheric transport models such as in SiBcrop-RAMS (Corbin et al., 2010), RAMS-Leaf3-5PM (Tolk et al., 2009), and WRF-VPRM (Ahmadov et al., 2007). The next generation of vegetation and atmospheric models integrates both perspectives in two-way interacting land–atmosphere models, in which carbon from the atmosphere is accumulated into vegetation, which in turn feeds back energy, water, and CO<sub>2</sub> to the atmosphere overhead (e.g. the C<sup>4</sup>MIP models HadCM3LC, IPSL-CM4-LOOP, Bern-CC in Cox et al., 2013; Friedlingstein et al., 2006).

Recent studies have analyzed the underlying mechanisms of land–atmosphere interactions and feedbacks, using two-way couplings between the land surface and the planetary boundary layer (Santanello et al., 2013; Mcgrath-Spangler and Denning, 2010; van Heerwaarden et al., 2009). Among them, Vilà-Guerau de Arellano et al. (2012) have clearly demonstrated the importance of how these interactions are described. They showed that future conditions of CO<sub>2</sub> level rise and warming would influence the boundary-layer cloudiness by affecting the plant stomatal aperture and vapor pressure deficit (VPD), thus changing both evapotranspiration and atmospheric humidity. Upper atmosphere conditions, which are connected to large-scale synoptic weather patterns, were suggested to further affect the stomatal response through their control on diurnal boundary-layer growth and entrainment. Although the Vilà-Guerau de Arellano et al. study only focused on the diurnal and local scale with a relatively simple coupled model, the implications for two-way coupled models operating on much larger and longer scales was evident.

In this study, we continue this approach and analyse the coupling between the heat, moisture and carbon cycles for a maize field. We specifically focus on the diurnal scale, like Vilà-Guerau de Arellano et al. (2012), paying particular attention to the simulation of carbon fluxes, and especially photosynthesis, which have a cumulative impact on

## Two perspectives on coupled exchange in the boundary layer

M. Combe et al.

Title Page

Abstract

Introduction

Conclusions

References

Tables

Figures



Back

Close

Full Screen / Esc

Printer-friendly Version

Interactive Discussion



crop growth and crop yield at the seasonal scale. We also explore the relative importance of upper atmosphere conditions like subsidence, compared to the role of surface forcings like soil moisture, for the determination of CO<sub>2</sub> mole fractions. We choose to focus on crop-atmosphere interactions because croplands occupy a fifth of the European Union land surface (FAOSTAT 2011 land-use statistics) and are important for food production, but are often not well represented in land-surface models. In Dynamic Global Vegetation Models (DGVM), and in Soil–Vegetation–Atmosphere Transfer models (SVAT models), they are conceptualized either as natural (e.g. Sitch et al., 2003) or managed grass (e.g. Krinner et al., 2005), and only distinguished by C<sub>3</sub> or C<sub>4</sub> plant photosynthesis. Differences between species of crops in development are often not simulated, but are prescribed using seasonal leaf area index (LAI). Also, nitrogen stress or the effect of management options (fertilization, irrigation, plowing) are often not implemented at all, while they have been shown to have large impact on crop carbon cycling (Ciais et al., 2010; Lehuger et al., 2010; Gervois et al., 2008). In contrast to DGVMs, process-based crop models potentially represent these crop characteristics better (Challinor et al., 2009; Betts, 2005).

In order to investigate the differences between these two contrasting representations of crop biology, we use a process-based crop yield forecast model, GECROS (Yin and van Laar, 2005), and a more meteorological-oriented, plant surface–atmosphere exchange model, A-g<sub>s</sub> (Ronda et al., 2001). We couple them to the same atmospheric model and compare their ability to reproduce crop-atmosphere interactions. Both models simulate the diurnal carbon, water and heat surface fluxes, with A-g<sub>s</sub> more focussed on representing the individual surface energy balance terms. The additional levels of complexity embedded in GECROS are the separation of the effects of diffuse and direct radiation on photosynthesis, the internal calculation of crop LAI, the allocation and storage of carbon into crop organs (leading to crop yield), and the interaction of the carbon and nitrogen cycles (nitrogen stress). We assess both models using a very comprehensive observational dataset from a maize field in the Netherlands (Jans et al., 2010), that includes atmospheric variables (temperature, humidity, radia-

tion), the surface fluxes of CO<sub>2</sub>, water and (sensible and ground) heat, the soil temperature and humidity, as well as the seasonal crop development (crop height, LAI, dry matter weight). We combine it with boundary-layer height data from a nearby meteorological station (Cabauw experimental site for atmospheric research, online database available at <http://www.cesar-database.nl>). It is important to stress that these observations were conducted at the same local scale as we simulate (field scale), which is smaller than typically simulated in climate models (i.e. 50 km resolution at minimum). In order to bridge these different scales (Eitzinger et al., 2008; Betts, 2005), we couple both our surface models, GECROS and A-g<sub>s</sub>, to a model for the atmospheric boundary layer. This framework enables us to draw conclusions about the key boundary layer-vegetation interactions, and we use it to answer two research questions:

1. What are the essential processes at the surface and upper atmosphere governing the coupled carbon, water and energy budgets of the crop-atmosphere system?
2. What is the level of complexity needed for a plant physiology model to correctly reproduce the interactions of a cropland with the atmosphere?

The next section presents a description of our surface and atmospheric models, as well as of their coupling method. It also introduces the design of two sensitivity analyses, which aim at showing the importance of upper atmospheric conditions in the crop-atmosphere system. We then start our Results section with an insight into the state-of-the-art, carbon-storage perspective on the surface exchange, and a short seasonal sensitivity analysis of its one-way crop-atmosphere interactions. We then present the core of our findings, with the full diurnal intercomparison of our two coupled models against observations, and a sensitivity analysis of the two-way diurnal crop-atmosphere interactions.

## BGD

11, 5275–5325, 2014

### Two perspectives on coupled exchange in the boundary layer

M. Combe et al.

Title Page

Abstract

Introduction

Conclusions

References

Tables

Figures



Back

Close

Full Screen / Esc

Printer-friendly Version

Interactive Discussion



## 2 Methods

### 2.1 Observations

In order to verify the behavior of the cropland–atmosphere system, we use a comprehensive set of surface exchange, atmosphere, soil and crop growth observations, which were performed in 2007 and 2008 at a maize field located in Wageningen, the Netherlands (see Jans et al., 2010). This dataset consists of half-hourly averages of the sensible and latent heat fluxes, and of CO<sub>2</sub> exchange, obtained with the eddy covariance (EC) technique, and quality-controlled, according to the protocols described in Aubinet et al. (2012). These EC observations are supported by various continuous micrometeorological measurements in the air and in the soil. In addition to the continuous measurements, this dataset includes soil type, crop management data, as well as intermittent observations of crop height, plant area index – i.e. a proxy for LAI – and the dry weight of crop organs over the growing season. To complete the atmospheric observations from Jans et al., we use the boundary-layer height from the wind profiler measurements of the closest meteorological station, Cabauw, the Netherlands, located approximately 50 km West from the maize site (Cabauw experimental site for atmospheric research, online database available at <http://www.cesar-database.nl>). In the absence of boundary-layer height data for Wageningen, this is the best estimation possible.

The continuous measurements show an energy gap in the surface energy balance, between the net absorbed radiation and the sum of the surface (latent, sensible, ground) heat fluxes. This energy gap is typical for a crop like maize, due to heat storage, photosynthesis – which can proceed at unusually large rates for maize, large-scale heat transport processes, and in a lesser extent to measurement accuracy (Meyers and Hollinger, 2004; Foken et al., 2010). But because the two surface schemes we use assume the closure of the surface energy budget, we allocate the missing energy into extra sensible and latent heat in the observations, using the Bowen ratio to deter-

**BGD**

11, 5275–5325, 2014

## Two perspectives on coupled exchange in the boundary layer

M. Combe et al.

Title Page

Abstract

Introduction

Conclusions

References

Tables

Figures



Back

Close

Full Screen / Esc

Printer-friendly Version

Interactive Discussion



mine the partitioning. This correction method has been previously used by Twine et al. (2000).

Because we want to focus on the diurnal scale to study the interactions and feedbacks of our maize-atmosphere system, we specifically pick one day of observations, the 4 August 2007, which was a sunny, cloudless day, and with a convective atmospheric boundary layer above the maize field. We pick that specific date because our atmospheric boundary-layer model can only reproduce well-mixed boundary layers, but also because we want to avoid sensitive periods of emergence and senescence times for the crop. On the 4 August 2007, our maize crop is in the reproductive stage, at the peak of its growth (see LAI in Fig. 1).

## 2.2 Models

In order to study the diurnal cropland-atmosphere system, we couple two surface schemes, GECROS and A-g<sub>s</sub>, to a convective atmospheric boundary-layer scheme, MXL, and analyse their behavior compared to our observations for the 4 August 2007.

### 2.2.1 MXL, a convective atmospheric boundary-layer scheme

Our atmospheric boundary-layer scheme is a mixed-layer model, which describes accurately the development of the diurnal atmospheric boundary layer (ABL) when turbulence is strong. First studies to develop the concept of a mixed-layer model were done by Lilly (1968); Betts (1973); Carson (1973) and Tennekes (1973). The version used in this paper has been described by Vilá-Guerau de Arellano et al. (2009). During this daytime, strongly convective regime, the ABL is well-mixed, thus we consider the instantaneous atmospheric variables assume a single value throughout the whole ABL. The top of the boundary layer is characterized by temperature, moisture and CO<sub>2</sub> inversions, simplified as sudden “jumps” or gradients, which sharply separate the ABL state from the free tropospheric profiles. The evolution of the ABL state and height over time is determined by boundary fluxes (surface, entrainment and advection) of heat, mois-

**BGD**

11, 5275–5325, 2014

## Two perspectives on coupled exchange in the boundary layer

M. Combe et al.

Title Page

Abstract

Introduction

Conclusions

References

Tables

Figures

◀

▶

◀

▶

Back

Close

Full Screen / Esc

Printer-friendly Version

Interactive Discussion



ture and CO<sub>2</sub>. The MXL model has been widely tested and is a robust model for sunny days with few to no boundary-layer clouds, all conditions met by the 4 August 2007 over our maize field.

## 2.2.2 GECROS, a crop yield forecast model

5 The Genotype-by-Environment interactions on CROp growth Simulator (GECROS) version 1.0 is a generic process-based crop yield forecast model released by Yin and van Laar (2005). GECROS is from the two-big leaf family of models initiated by De Pury and Farquhar (1997), which means the crop canopy is simplified as two leaves possessing each one sub-stomatal cavity. One leaf represents the entire sunlit leaf area of  
10 the canopy, the other represents the entire shaded leaf area, their proportions evolving with crop age and solar angle. The two big-leaves work in parallel for diurnal photosynthetic and transpiration processes. This enables different efficiencies of photosynthesis to happen under diffuse and direct radiation.

On the diurnal scale, GECROS is a crop growth model based on evaporative demand, which means that the potential photosynthesis is first calculated according to the amount of available photosynthetically active radiation, and then it determines the leaf conductance and the potential transpiration. The actual photosynthesis and transpiration are obtained by checking the soil water balance: if the water supply is sufficient for potential transpiration, GECROS works at full potential level. Otherwise, GECROS  
15 transpires solely the available water supply, and reduces its photosynthesis and conductance accordingly. In addition to water stress, GECROS has a diurnal nitrogen cycle implemented that interacts with the carbon cycle, accounting for nitrogen stress. This last feature did not play a role in our study of crop-atmosphere interactions on the 4 August 2007.

25 On the seasonal scale, GECROS simulates its own phenological development based on the accumulation of heat (i.e. growing degree-days). Also, it accumulates carbon into the different crop organs (leaves, stems, roots and storage organs), which determines crop yield. Both of these features, typical of a crop model but not of a DGVM or

## Two perspectives on coupled exchange in the boundary layer

M. Combe et al.

Title Page

Abstract

Introduction

Conclusions

References

Tables

Figures



Back

Close

Full Screen / Esc

Printer-friendly Version

Interactive Discussion



SVAT model, allow interactions and feedbacks between the crop and the atmosphere to change with crop ageing. This is a potential advantage for a seasonal study of the cropland–atmosphere system.

### 2.2.3 Modifications to GECROS used in this paper

We analyzed the surface energy budget of GECROS and identified two core problems in its original version: (a) the budget of net longwave radiation was faulty, generating too much outgoing longwave radiation and consequently too little energy to be retained at the surface, and (b) the calculated VPD was too high because it used the humidity at 2 m instead of inside-canopy humidity, stimulating latent heat too much at the expense of sensible heat. In order for GECROS to have realistic heat fluxes to feed to the MXL model, we implemented the following changes to improve its surface energy balance. First, we replaced the original net longwave radiation budget by a simplified multilayer budget:

$$LW_i = \left( \underbrace{\mathcal{E}_{ATMOS} \times \sigma \times T_{ATMOS}^4}_{\text{Incoming radiation}} - \underbrace{\mathcal{E}_i \times \sigma \times T_i^4}_{\text{Outgoing radiation}} \right) \times F_i \quad (1)$$

$$\text{with } F_i = \begin{cases} f_{veg} & \text{if sunlit leaf } (i = 1) \\ 0 & \text{if shaded leaf } (i = 2) \\ 1 - f_{veg} & \text{if bare soil } (i = 3) \end{cases}$$

$\mathcal{E}_{ATMOS}$  and  $\mathcal{E}_i$  are emissivities,  $T_{ATMOS}$  and  $T_i$  are temperatures,  $\sigma$  is the Stefan–Boltzmann constant and  $f_{veg}$  is the vegetation cover fraction. We assume similar blackbody radiation ( $\mathcal{E}_1 = \mathcal{E}_2 = \mathcal{E}_3 = 1$ ) originating from the sunlit-, shaded-leaf and the underlying soil. As a consequence, we approximate the net longwave radiation budget of the shaded leaf to be zero. This approximation for shaded leaves in a multilayer model is supported by Zhao and Qualls (2006).

## Two perspectives on coupled exchange in the boundary layer

M. Combe et al.

Title Page

Abstract

Introduction

Conclusions

References

Tables

Figures

◀

▶

◀

▶

Back

Close

Full Screen / Esc

Printer-friendly Version

Interactive Discussion



## Two perspectives on coupled exchange in the boundary layer

M. Combe et al.

Title Page

Abstract

Introduction

Conclusions

References

Tables

Figures

◀

▶

◀

▶

Back

Close

Full Screen / Esc

Printer-friendly Version

Interactive Discussion



Then, in order to decrease the allocation of energy into the latent heat flux, we create a ground heat flux (it was assumed negligible in the original GECROS version). We take a first-order estimate and parameterize it to be 10 % of the net absorbed radiation at the surface (this assumption was validated for short grass by de Bruin and Holtslag, 1982).

Finally, we implement a vapor pressure profile in the canopy layer to enable a more realistic description of VPD. In our implementation, the vapor pressure ( $e$ ) changes linearly from top to bottom of the canopy, from the actual vapor pressure at 2 m to the saturation vapor pressure at 2 m. The state of saturation at bottom of the canopy is adjusted for cases of lighter vegetation cover. This allows the vapor pressure at the bottom to be always larger or equal to  $e(2\text{m})$ .

$$e(z) = e(2\text{m}) + (e_0 - e(2\text{m})) \times d_{\text{rel}} \quad (2)$$

$$\text{with } e_0 = e(2\text{m}) + (e_{\text{SAT}}(2\text{m}) - e(2\text{m})) \times f_{\text{veg}}$$

We use the relative canopy depth  $d_{\text{rel}} = 0.5$  for shaded leaves and  $d_{\text{rel}} = 0.9$  for the soil. Note that, combined to the canopy profile for vapor pressure, we do not implement a canopy profile for air temperature. We keep air temperature vertically constant and equal to the 2 m air temperature. We refer to the modified version of the GECROS model from here on.

### 2.2.4 A- $g_s$ , a land-surface exchange model

The A- $g_s$  model is a single big-leaf model that relates plant  $\text{CO}_2$  assimilation to the stomatal conductance ( $g_s = 1/r_s$ ) via a  $\text{CO}_2$  gradient (see Eq. 3). We use the version of Ronda et al. (2001), where the impact of soil water depletion on  $g_s$  is calculated with a linear function from wilting point to field capacity. In Eq. (3), soil respiration is computed with an Arrhenius-type equation, using the concepts of reference respiration  $R_{10}$  and of the activation energy for chemical reactions  $E_a$ . In addition to the  $\text{CO}_2$  fluxes, A- $g_s$  calculates surface fluxes of latent and sensible heat with the same conductance approach (see Eqs. 4–5). Finally, the ground heat flux is calculated as the thermal

diffusivity of the skin layer times the temperature difference between the soil and skin layers.

$$\underbrace{(\overline{w'c'})_s}_{\text{Net ecosystem exchange}} = \underbrace{\left(\frac{1}{r_a + 1.6 r_s}\right)}_{\text{CO}_2 \text{ conductance}} \times \underbrace{(c_{\text{stomata}} - c_{\text{atmos}})}_{\text{CO}_2 \text{ gradient}} + \text{Soil Respiration} \quad (3)$$

$$\underbrace{(\overline{w'q'})_s}_{\text{Surface moisture flux}} = \underbrace{\left(f_{\text{veg}} \times \frac{1}{r_a + r_s} + (1 - f_{\text{veg}}) \times \frac{1}{r_a + r_{\text{soil}}}\right)}_{\text{water conductance}} \times \underbrace{(q_{\text{sat}}(T_{\text{skin}}) - q_{\text{atmos}})}_{\text{moisture gradient}} \quad (4)$$

$$\underbrace{(\overline{w'\theta'})_s}_{\text{Surface heat flux}} = \underbrace{\left(\frac{1}{r_a}\right)}_{\text{heat conductance}} \times \underbrace{(T_{\text{skin}} - \theta_{\text{atmos}})}_{\text{temperature gradient}} \quad (5)$$

A-g<sub>s</sub> adapts its surface fluxes according to the vegetation cover and LAI, but simulates neither its own crop phenological development nor carbon accumulation into crop organs. This set-up makes the A-g<sub>s</sub> model, in the present version, suited for the simulation of surface exchanges at the diurnal scale only.

### 2.3 Simulation setup

We use the only model that can run on a seasonal scale, the uncoupled GECROS model, to simulate the day-to-day variations of the carbon, water and heat surface fluxes. We use it to gain insight into the carbon storage-oriented view of the land surface exchange. For this, we initialize the GECROS model with the maize parameters of Yin and van Laar (2005) and Sinclair and de Wit (1975) (cf. Table A3). The uncoupled GECROS is run from emergence date to maturity date. The results of this uncoupled simulation are presented in Sect. 3.1.

## BGD

11, 5275–5325, 2014

### Two perspectives on coupled exchange in the boundary layer

M. Combe et al.

Title Page

Abstract

Introduction

Conclusions

References

Tables

Figures

◀

▶

◀

▶

Back

Close

Full Screen / Esc

Printer-friendly Version

Interactive Discussion



## Two perspectives on coupled exchange in the boundary layer

M. Combe et al.

Title Page

Abstract

Introduction

Conclusions

References

Tables

Figures

◀

▶

◀

▶

Back

Close

Full Screen / Esc

Printer-friendly Version

Interactive Discussion



Then with the three models presented before, we make two couplings to study the diurnal maize-atmosphere system: MXL-A-g<sub>s</sub> and MXL-GECROS. We design them as two-way couplings: the surface fluxes given by A-g<sub>s</sub> and GECROS are used as surface conditions for the MXL model, and in return, the incoming short wave radiation, atmospheric temperature, humidity, wind speed, and CO<sub>2</sub> mole fraction are fed to the surface schemes as environmental conditions. The internal calculations of MXL are done on a time step of one minute. In addition, A-g<sub>s</sub> and GECROS do their own internal calculations and communicate with MXL on time steps of respectively 1 and 5 min. These calculations start at 06:00 UTC, after sunrise and when convection is already active, and last until 18:00 UTC. The main settings of our models are presented in Tables A1–A3. In the case of MXL-GECROS, we use the uncoupled simulation of GECROS, presented above, to lead the crop to the developmental stage before we activate the two-way coupling on 4 August. On that day, we initialize all our models following the available soil, crop and atmospheric observations from Jans et al. (2010). In addition, we use the C<sub>4</sub> photosynthesis parameters published by Ronda et al. (2001) to initialize the A-g<sub>s</sub> scheme.

The dataset from Jans et al. (2010) provides the soil volumetric water content on the 4 August 2007, but no precise estimate for the soil wilting point and field capacity at the maize site. As a consequence, we choose to use the meteorological-oriented model, MXL-A-g<sub>s</sub>, to adjust the initial soil moisture within the boundaries of rough estimates for the wilting point and field capacity, in order to obtain the observed Bowen ratio (ratio of sensible to latent heat flux). In the model, this regulation of the Bowen ratio with soil moisture is caused by the occurrence of water-stress, which happens linearly between wilting point and field capacity. After the adjustment of soil moisture, we obtain a soil moisture index of 55.5 % (SMI gives the relative position of the actual soil moisture in between the wilting point and field capacity, see Eq. 6).

$$\text{SMI} = \frac{W_{\text{actual}} - W_{\text{wilting point}}}{W_{\text{field capacity}} - W_{\text{wilting point}}} \quad \text{with } W \text{ the soil volumetric water content} \quad (6)$$

## Two perspectives on coupled exchange in the boundary layer

M. Combe et al.

Title Page

Abstract

Introduction

Conclusions

References

Tables

Figures



Back

Close

Full Screen / Esc

Printer-friendly Version

Interactive Discussion



The absolute soil volumetric water content values used to calculate this SMI are placed in the Tables A2 and A3. We regard this SMI of 55.5 % as a reasonable estimate, considering the observed soil moisture on the 4 August 2007 and the range of variations of soil moisture over the year. We apply the same wilting point, field capacity, and soil moisture for MXL-GECROS. Thus both models operate with the same realistic soil type, absolute soil moisture and SMI, but they will yield different Bowen ratios and surface energy balances because of the different water stress implementation in the two models (GECROS experiences no water-stress above SMI 11 %).

In the absence of observations for soil respiration on the 4 August 2007, we adjust the MXL-A- $g_s$  soil respiration to be identical to the internally calculated value from MXL-GECROS ( $0.2 \text{ mg CO}_2 \text{ m}^{-2} \text{ s}^{-1}$  at 12:00 UTC). This means that for the net ecosystem exchange (NEE), the only difference between the two models is in their representation of net primary production (NPP). We execute this by setting the reference respiration  $R_{10}$  of MXL-A- $g_s$  at  $0.03 \text{ mg CO}_2 \text{ m}^{-2} \text{ s}^{-1}$ , a low but realistic number when considering the natural range of variation of  $R_{10}$  in the Netherlands (cf. Jacobs et al., 2007). Also, the estimate of soil respiration is in the range of observed values at that period of the year (Jans et al., 2010).

Finally, in order to obtain the same input of shortwave radiation as in our observations ( $25.0 \text{ MJ m}^{-2}$ ) on the 4 August 2007, we prescribe a cloud cover of 22.5 % in our models to match the observed total incoming short wave radiation (SWin) during daytime. This is because the observations show a significant reduction of SWin compared to the output of astronomic functions for a cloudless day, likely due to haze or fog in the morning. With our two coupled models, we make an intercomparison of their simulations against observations, to study the ability of these couplings to reproduce the cropland–atmosphere interactions.

## 2.4 Sensitivity analyses

We perform two different sensitivity analyses in this study. We first want to show the importance of changes in synoptic weather patterns for crop-atmosphere interactions.

## Two perspectives on coupled exchange in the boundary layer

M. Combe et al.

Title Page

Abstract

Introduction

Conclusions

References

Tables

Figures

◀

▶

◀

▶

Back

Close

Full Screen / Esc

Printer-friendly Version

Interactive Discussion



We analyse the integrated consequences of these changes on the seasonal scale with the help of a carbon-storage model, the uncoupled GECROS model, where the crop-atmosphere interactions are conceptualized as one-way interactions. We use the GECROS control run as defined in Sect. 2.3 to generate 100 simulations. In each simulation, we take the weather of the control case, and randomly vary the sequence of days within periods of 30 days (we thus divide the year into 12 periods of 30 days and 1 period of 5 days). This creates a year of weather that is similar to the control one (same averages, standard deviations and sums of solar radiation, precipitation, temperature, wind and humidity) and which respects the seasonal evolution of the weather, but in which the timing of synoptic weather events is randomized within a month. We analyse the impact of these changes in synoptic weather patterns on the dry matter yield of the crop.

In addition, and related to our main goals, we evaluate the sensitivity of the diurnal cropland–atmosphere system to upper atmospheric conditions (subsidence) in comparison to surface conditions (soil moisture). We conduct this sensitivity analysis with the model that shows the best performance on the diurnal scale (i.e. MXL-A-g<sub>s</sub>, see Results). We design two study cases, stemming from the control case of the 4 August 2007 of Sect. 2.3, by selecting two drivers to modify separately: (a) the “high subsidence” case, where we replace the very small horizontal wind divergence ( $7 \times 10^{-6} \text{ s}^{-1}$ ) of the control case by a high one ( $4 \times 10^{-5} \text{ s}^{-1}$ ), representing a realistic case of strong subsidence in the Netherlands, and (b) the “soil moisture depletion” case, where we apply a reduction of soil moisture (from  $0.110$  to  $0.105 \text{ cm}^3 \text{ cm}^{-3}$ ), equivalent to a 5% decrease of SMI for that soil type. A decrease of 5% SMI could happen over several days in a drying phase (e.g. Daly et al., 2004; Betts, 2004). We analyse the impact of these two external forcings on the diurnal surface energy balance and NEE, as well as the net effect on the atmospheric  $\text{CO}_2$  mole fraction.

### 3 Results

#### 3.1 The carbon-storage perspective on land surface exchange

Figure 1 presents the typical carbon-storage view of the land surface, as seen in crop yield forecasts. We show three integrative variables evolving over the growing season: yield, plant area index and crop height. In Fig. 1a, we find that the GECROS model reproduces the observed maize yield at day 282 within 10% ( $2 \text{ kg m}^{-2}$  simulated vs.  $1.8 \text{ kg m}^{-2}$  observed), indicating a correct integration of NPP over the growing season. Moreover, Fig. 1b and c show that GECROS also approaches the observed maximum plant area index (PAI) – a proxy for LAI – and crop height, with a  $3.5 \text{ m}^2 \text{ m}^{-2}$  PAI and a 2.5 m height vs. an observed  $3.8 \text{ m}^2 \text{ m}^{-2}$  PAI and 2.8 m height. This suggests that the NPP was also assigned to the correct GECROS carbon pools (stems, leaves, roots) during crop development. This satisfactory agreement for carbon storage was expected and is reassuring, since the GECROS model was built as a crop yield model (Yin and van Laar, 2005). It is additionally interesting to analyse how the uncoupled GECROS model simulates day-to-day variations of surface fluxes of carbon, energy and water, in order to understand how it will feed back on the atmosphere in a full coupling with MXL.

Figure 2 presents an unusual view of crop growth models, as it shows the seasonal evolution of surface available energy ( $Q_{\text{net}}$ ), latent heat flux (LE), sensible heat flux (SH) and net  $\text{CO}_2$  exchange (i.e. NEE) in daily integrated amounts. Their seasonal means, presented in Table 1, are all in good agreement with the observations, except for a small overestimation of the mean NEE. This overestimation could be due to a too low soil respiration. Also, the  $R^2$  between the modelled and observed daily integrated  $Q_{\text{net}}$  (0.95) is very high, and the  $R^2$  for the daily integrated LE (0.75), SH (0.59) and NEE (0.74) are satisfactory. The high degree to which GECROS reproduces the variability from day-to-day results from the prescribed meteorological driver data in the seasonal simulation, which provides the model with observed radiation, atmospheric temperature, and precipitation data. Note that the mismatch between observations and

BGD

11, 5275–5325, 2014

Two perspectives on coupled exchange in the boundary layer

M. Combe et al.

Title Page

Abstract

Introduction

Conclusions

References

Tables

Figures

◀

▶

◀

▶

Back

Close

Full Screen / Esc

Printer-friendly Version

Interactive Discussion



GECROS on individual days can nevertheless be quite large (cf. the RMSE compared to the observed seasonal means and standard deviations in Table 1), despite the improvements we made to its energy balance (see Methods). This suggests that two-way interactions on the diurnal scale, not represented in the uncoupled GECROS model, might have an additional strong control over the daytime fluxes. This reinforces the aim of our study, which is to focus on understanding the diurnal two-way crop-atmosphere interactions.

Finally, in order to demonstrate the importance of large-scale atmospheric conditions for the crop-atmosphere system, we present, in Fig. 3, the sensitivity of crop yield to the synoptic weather patterns. We find that in 91 % of the cases, the yield varies around the control yield (in red) with a spread of  $0.5 \text{ kg m}^{-2}$ , which represents 25 % of the original yield. This shows that variations in the sequence of synoptic weather events can generate significant changes in daily NPP, which then strongly impact yield. In addition, if we account for the remaining 9 % of the cases, which is composed of extremely low yields, we find that the crop yield can actually vary within a total range of  $1.7 \text{ kg m}^{-2}$ , which represents 85 % of the original yield. Those 9 % cases show that such changes in the sequences of weather events can actually cause the failure of crop growth, because of unfavorable sequences of weather situations during the establishment of the crop (the slope of the linear increase in total dry matter during the vegetative growth is set during the first month of crop development). This shows that there might be more sensitive periods of crop development during which the impact of large-scale atmospheric conditions become truly critical. We investigate the diurnal crop-atmosphere interactions next using the two land-surface models coupled to the mixed-layer on minute time-scales, to see which underlying processes are important.

## BGD

11, 5275–5325, 2014

### Two perspectives on coupled exchange in the boundary layer

M. Combe et al.

Title Page

Abstract

Introduction

Conclusions

References

Tables

Figures



Back

Close

Full Screen / Esc

Printer-friendly Version

Interactive Discussion



## 3.2 Intercomparison of coupled models against observations

### 3.2.1 Diurnal evolution of the surface fluxes

Figure 4 presents three of the four components of the surface energy balance, together with the net surface CO<sub>2</sub> exchange, for the 4 August 2007. As shown in Fig. 4, both MXL-GECROS and MXL-A-g<sub>s</sub> calculate reasonable magnitudes and temporal evolutions of the surface fluxes for the observed maize crop, but MXL-A-g<sub>s</sub> performs slightly better than MXL-GECROS. We find in Fig. 4a that both models calculate different amounts of Qnet. They benefit from the same amount of incoming shortwave radiation (25.0 MJ m<sup>-2</sup> integrated over the day), but yield different radiation balances, since they have differently parameterized functions for albedo and longwave radiation budgets of the leaves and soil. As a result, a different amount of available energy will be partitioned into sensible heat, latent heat and ground heat fluxes. Following Qnet, in Fig. 4b–d, we find that, integrated between 06:00 UTC and 18:00 UTC, MXL-GECROS underestimates SH by a total of 1.3 MJ m<sup>-2</sup> (30 %), and overestimates LE by 2.9 MJ m<sup>-2</sup> (31 %) and NEE by 16.5 g CO<sub>2</sub> m<sup>-2</sup> (30 %, see Table 2). On the other hand, MXL-A-g<sub>s</sub> agrees satisfactorily with both SH and LE, but underestimates NEE by a total of 9.0 g CO<sub>2</sub> m<sup>-2</sup> (16 %). Considering the three fluxes of heat, water and CO<sub>2</sub>, we find that MXL-A-g<sub>s</sub> reproduces the observed diurnal evolution of the surface fluxes better than MXL-GECROS on the 4 August 2007. It is important to remember that we prescribe the initial soil moisture to match the observed Bowen ratio with MXL-A-g<sub>s</sub>, which is why we arrive at this better fit for the surface energy balance of this model. We prescribe the same SMI (55.5 %) to both models, which have different water-stress responses, hence the lesser fit for MXL-GECROS.

In Fig. 4a, we identify three phases in the observed surface fluxes diurnal cycle. Phase A corresponds to the early morning transition from a stable to a convective boundary layer. During Phase A, the SH flux switches from negative to positive, and this heat becomes the source of convection which works to break up the thermal strat-

BDG

11, 5275–5325, 2014

Two perspectives on coupled exchange in the boundary layer

M. Combe et al.

Title Page

Abstract

Introduction

Conclusions

References

Tables

Figures

◀

▶

◀

▶

Back

Close

Full Screen / Esc

Printer-friendly Version

Interactive Discussion



ification built during nighttime. Reproducing this observed transition with our models is difficult. First of all, because advection of heat and moisture plays an important role in this early morning phase (see next section), but also dew on the vegetation has possibly delayed the onset of a positive SH. Therefore, we will not discuss the timing of the early morning transition further.

Phase B is the most important part of the day, when fluxes are highest and convection is strong. During Phase B, MXL-GECROS is strongly underestimating SH, in accordance with its consistently higher LE flux. Due to the coupling with evapotranspiration, photosynthesis is overestimated as well, as shown in NEE (considering that the soil respiration is low and identical between MXL-GECROS and MXL-A-g<sub>s</sub>). These strong fluxes contribute most to the daily integrated amount, which impact the atmospheric state. Therefore it is very important to calculate correct surface fluxes during Phase B, which MXL-A-g<sub>s</sub> does better than MXL-GECROS.

Finally, Phase C is the the late afternoon transition from a convective to a stable boundary layer. During Phase C, the SH flux changes from positive to negative, causing the convection to cease. Also, evapotranspiration and photosynthesis are decreasing until fluxes are becoming negligible. The late afternoon transition for SH occurs much earlier for MXL-GECROS (15:00 UTC) than for MXL-A-g<sub>s</sub> (17:00 UTC) and the observations (18:00 UTC), which means the assumption of a convective boundary layer, the basis of the MXL model, ends earlier for MXL-GECROS than for MXL-A-g<sub>s</sub>. To see how the differences in magnitudes and timing of heat, water, and carbon surface fluxes impact the atmospheric state, we assess the atmospheric mixed-layer next.

### 3.2.2 Diurnal evolution of the atmospheric boundary layer

Figure 5 presents the diurnal evolution of the atmospheric temperature, specific humidity, CO<sub>2</sub> mole fraction and boundary-layer height. When comparing observations with the model results, note that we present the modelled mixed-layer (or bulk) values against the 2 m observations for temperature and specific humidity. Considering the general properties of the surface layer, the observed atmosphere is thus expected to

**BGD**

11, 5275–5325, 2014

## Two perspectives on coupled exchange in the boundary layer

M. Combe et al.

Title Page

Abstract

Introduction

Conclusions

References

Tables

Figures

⏪

⏩

◀

▶

Back

Close

Full Screen / Esc

Printer-friendly Version

Interactive Discussion



## Two perspectives on coupled exchange in the boundary layer

M. Combe et al.

Title Page

Abstract

Introduction

Conclusions

References

Tables

Figures



Back

Close

Full Screen / Esc

Printer-friendly Version

Interactive Discussion



be slightly warmer and moister than the modelled atmosphere. Also, because the negative SH depletes the layer of air close to the surface from heat at the very end of the day, the observed 2 m temperature is expected to decrease at that time. Keeping these expected differences in mind, we find that the MXL-A- $g_s$  model reproduces the observed temperature and moisture values well, while MXL-GECROS calculates a clearly too high 18:00 UTC humidity ( $11.2 \text{ g kg}^{-1}$ ) compared to the observations ( $9.8 \text{ g kg}^{-1}$ ). Similarly, MXL-GECROS simulates a too  $\text{CO}_2$ -depleted atmosphere ( $-20 \text{ ppm}$ ) and a too shallow boundary layer ( $-250 \text{ m}$ ) compared to observations, where MXL-A- $g_s$  performs relatively well. This indicates that MXL-A- $g_s$  outperforms MXL-GECROS on the diurnal scale, when a full crop-atmosphere coupling is established.

When we relate the integrated heat, water and  $\text{CO}_2$  surface fluxes of Table 2 to the atmosphere of Fig. 5, we observe, as expected, that a lower integrated amount of SH in MXL-GECROS compared to MXL-A- $g_s$  leads to a  $2^\circ\text{C}$  lower maximum temperature ( $24$  instead of  $26^\circ\text{C}$ ). Also, a higher integrated LE in MXL-GECROS compared to MXL-A- $g_s$  results in a  $1.4 \text{ g kg}^{-1}$  higher specific humidity at end of the day ( $11.1$  instead of  $9.7 \text{ g kg}^{-1}$ ). Finally a lower integrated NEE in MXL-GECROS compared to MXL-A- $g_s$  leads to a  $22 \text{ ppm}$  lower  $\text{CO}_2$  mole fraction ( $333$  instead of  $355 \text{ ppm}$ ). But when we compare the modelled and observed atmosphere, we find discrepancies. This is because surface fluxes do not directly translate into a diurnal evolution of the atmospheric temperature, humidity and  $\text{CO}_2$  mole fraction. For instance, in Fig. 5c, we find that the daytime overestimation of NEE by MXL-GECROS leads to a too strongly  $\text{CO}_2$ -depleted atmosphere compared to observations only in the afternoon. Also for MXL-A- $g_s$ , despite a daytime underestimated NEE, it reproduces satisfactorily the observed  $\text{CO}_2$  daily minimum on 4 August 2007. This shows that errors in the surface fluxes can be canceled by other non-local effects like the advection, entrainment or boundary-layer dilution (e.g. see the role of dry-air entrainment in van Heerwaarden et al., 2009, or  $\text{CO}_2$  advection in Casso-Torralba et al., 2008). A full analysis of the diurnal cycle of the atmosphere must thus include the contribution of these processes.

Advection fluxes can change the expected evolution of the atmosphere. The occurrence of heat and moisture advection on the 4 August 2007 is noticeable because the observed diurnal range in temperature and the early morning increase in humidity are too large to be solely due to realistic crop sensible heat and evapotranspiration fluxes. We thus prescribed heat and moisture advection during the first hours of our numerical experiments. We estimate, for the MXL-A- $g_s$  model, that the contribution of advection to the diurnal temperature range (DTR, 13 °C) to be of 3 °C, and the contribution to the early morning specific humidity increase (1.8 g kg<sup>-1</sup>) to be of 1.2 g kg<sup>-1</sup>. The observed CO<sub>2</sub> mole fraction stabilization and increase after 13:00 UTC is also most probably generated by advection as well because an increase in CO<sub>2</sub> mole fraction could only be due to: (a) a positive NEE (which we do not have), (b) strong entrainment of CO<sub>2</sub>-rich air (which is unlikely at the end of the day), or (c) CO<sub>2</sub> advection. Despite this observation, we prescribed no advection of CO<sub>2</sub> in our model runs to more clearly demonstrate the role of surface fluxes in the CO<sub>2</sub> budget.

Finally, entrainment fluxes also alter the state of the boundary layer. The boundary-layer height ( $h$ ) of Fig. 5d can serve as a proxy for measuring the amount of warmer, drier, CO<sub>2</sub>-depleted air that is entrained from the free-troposphere into the boundary layer, in cases where there is no or very little subsidence (our case). In the end, we find in Fig. 5d that both models calculate maximum  $h$  that are lower (-150 m for MXL-A- $g_s$  and -250 m for MXL-GECROS) than observed (1400 m). Differences between the models are due to differences in heat input from SH and the subsequent entrainment, as the heat advection, free tropospheric vertical profiles and subsidence are identical between the models. But in reality, there are discrepancies in all of these variables, to create the existing differences between models and observations. Clearly, both boundary-layer dynamics and surface fluxes must be included in atmospheric simulations to properly capture the contribution of the large-scale air masses to the local atmospheric state. We will investigate the relevance of upper atmosphere conditions in more detail in the next section.

## Two perspectives on coupled exchange in the boundary layer

M. Combe et al.

Title Page

Abstract

Introduction

Conclusions

References

Tables

Figures



Back

Close

Full Screen / Esc

Printer-friendly Version

Interactive Discussion



### 3.3 Sensitivity analysis of an upper atmosphere forcing

We showed in the previous sections that MXL-A-g<sub>s</sub> performs best to reproduce the diurnal crop-atmosphere coupling on the 4 August 2007. As a consequence, we use it to conduct a sensitivity experiment. Our goal here is to quantify the strength of the couplings between the upper atmosphere, the boundary layer and the crop surface. From now on, we refer to the MXL-A-g<sub>s</sub> run of the previous sections as the control run, from which we derive our sensitivity analysis runs. We design two case studies: one where we apply a stronger upper atmosphere forcing (high subsidence) and another where we alter a land-surface forcing (depletion of soil moisture, see Sect. 2.4 for a detailed specification of the settings). Both high subsidence and soil moisture depletion are characteristic of a drought period. Figure 6 presents the main interactions between carbon, water, and energy that result in the state of the land-atmosphere. We use it to summarise the changes linked to increased subsidence, discussed in the next paragraphs.

While the high subsidence case stimulates the latent heat flux LE through the warming of the boundary layer (red arrows in Fig. 6), the soil moisture depletion case decreases LE through the closure of plant stomata. Subsidence is a large-scale forcing that counteracts the growth of the boundary layer and even reduces  $h$  once its growth has stopped (see the high subsidence case in Fig. 7a). It enhances the entrainment of warm free tropospheric air and causes a smaller volume of air to be warmed up by the same surface sensible heat flux, thus increasing the atmospheric temperature (+1.5 °C at 18:00 UTC, see Fig. 7b). This warming of the atmosphere increases the VPD at the surface and shifts the evaporative fraction ( $EF = LE / (SH + LE)$ ) towards evapotranspiration by 5% on average during the day (see Fig. 8a). Finally, this increase in LE results in a moistening of the atmosphere that counteracts the initial atmospheric drying caused by a short-term enhancement of dry-air entrainment (not shown here). In Fig. 7c we find that the specific humidity, which is first lower than in the control run, becomes higher than in the control run after 14:00 UTC due to the stimulation of LE.

BGD

11, 5275–5325, 2014

## Two perspectives on coupled exchange in the boundary layer

M. Combe et al.

Title Page

Abstract

Introduction

Conclusions

References

Tables

Figures

◀

▶

◀

▶

Back

Close

Full Screen / Esc

Printer-friendly Version

Interactive Discussion



## Two perspectives on coupled exchange in the boundary layer

M. Combe et al.

Title Page

Abstract

Introduction

Conclusions

References

Tables

Figures



Back

Close

Full Screen / Esc

Printer-friendly Version

Interactive Discussion



On the other hand, for the lower soil moisture case, the decreased availability of soil moisture generates a decrease in surface conductance  $g_s$  on average by  $1 \text{ mm s}^{-1}$  during the day (see Fig. 7d). This decrease in surface conductance leads to a reduction of EF of 5 % throughout the day (see Fig. 8a). As a result, we find that both cases affect the energy partitioning at the surface with equivalent magnitude. It is thus important to consider both the effect of high subsidence and soil moisture depletion on evapotranspiration in the context of drought response. Moreover, it is interesting to analyse how the net surface carbon uptake is affected by them.

High subsidence and soil moisture depletion have different impacts on the net  $\text{CO}_2$  flux at the surface. While the high subsidence case shows no difference in photosynthesis and respiration compared to the control case, the reduced soil moisture case presents a reduction in photosynthesis ( $-0.2 \text{ mg CO}_2 \text{ m}^{-2} \text{ s}^{-1}$  at midday in Fig. 9a). We relate this decrease of photosynthesis to the decrease in  $g_s$  ( $-1 \text{ mm s}^{-1}$ ) of Fig. 7d, which indicates a plant stomata closure in response to water stress. Thus, as a result of two very different feedback mechanisms on net photosynthesis and evapotranspiration (see previous paragraph), we obtain the same reduction in water use efficiency ( $\text{WUE} = -\text{NEE}/\text{LE}$ ) compared to the control case ( $-0.15 \text{ kg C kg H}_2\text{O}^{-1}$ , i.e.  $-4 \%$ , on average, see Fig. 8b). This means both forcings make carbon exchange, and by extension carbon storage, equally less water-efficient, which could impact yield in a drought situation. While a reduction in soil moisture has an immediate impact on the daily crop yield (integrated decrease of NPP of  $4.4 \text{ g CO}_2 \text{ m}^{-2}$ ), high subsidence does not. Nevertheless, in the previous paragraph we showed that the increased subsidence associated with high pressure systems could force the surface to evapotranspire more. High subsidence could thus aggravate soil moisture depletion over the days and ultimately contribute to a yield decrease. From a carbon cycle perspective, it is interesting to analyse in more detail how the atmospheric  $\text{CO}_2$  budget can be affected by surface and upper atmosphere modifications.

Figure 9 presents the atmospheric  $\text{CO}_2$  budget. In Fig. 9c, we see that the boundary-layer  $\text{CO}_2$  tendency receives equivalent contributions from the surface, and from en-

5 trainment, but their distribution in time differs. The contribution of entrainment to the overall CO<sub>2</sub> drawdown (−32 ppm in the control case) happens in the morning, before 09:00 UTC (i.e. 11:00 LT). On the other hand, the contribution of the surface uptake to the overall CO<sub>2</sub> drawdown (−34 ppm in the control case) is more constant throughout  
10 the day. In the high subsidence case, even though the entrainment of CO<sub>2</sub>-depleted air is lower (cf. Fig. 9b) and the NEE is unchanged (cf. Fig. 9a), both the surface and entrainment CO<sub>2</sub> tendencies are higher due to the lower boundary-layer volume (see Fig. 7a). This is because the tendencies are inversely proportional to the boundary-layer height in the mixed-layer framework, as shown by Pino et al. (2012). Consequently, the atmospheric CO<sub>2</sub> mole fraction is even more reduced in the high subsidence case (−12 ppm at 18:00 UTC relative to the control and soil moisture depletion cases, in Fig. 9d). Because the larger CO<sub>2</sub> drawdown is caused solely by the reduction in boundary-layer height in the high subsidence case, it is thus very important to consider the effect of increased subsidence in high pressure systems when interpreting  
15 measurements of the boundary-layer CO<sub>2</sub> mole fraction.

## 4 Discussion

In our study, we compare two coupled models, MXL-A-g<sub>s</sub> and MXL-GECROS, against a complete set of surface and boundary-layer observations. We show the importance of calculating surface fluxes of heat, water and CO<sub>2</sub> which interact with atmospheric conditions. This has been investigated for its expected improvement on numerical weather  
20 predictions (e.g. Boussetta et al., 2013; Moreira et al., 2013; Smallman et al., 2013; Hong et al., 2009), atmospheric CO<sub>2</sub> modelling (e.g. Corbin et al., 2010; Schuh et al., 2010; Tolk et al., 2009) and crop yield forecast (e.g. de Wit and Van Diepen, 2007). We agree with Smallman et al. (2013) that coupled models have high potential for the exploration of interactions and feedbacks within the land–atmosphere system (e.g. Santanello et al., 2013; Vilà-Guerau de Arellano et al., 2012; Davin et al., 2011; Subin et al.,  
25 2011; van Heerwaarden et al., 2010; Wramneby et al., 2010; Dirmeyer et al., 2006; Liu

**BGD**

11, 5275–5325, 2014

### Two perspectives on coupled exchange in the boundary layer

M. Combe et al.

Title Page

Abstract

Introduction

Conclusions

References

Tables

Figures

◀

▶

◀

▶

Back

Close

Full Screen / Esc

Printer-friendly Version

Interactive Discussion



## Two perspectives on coupled exchange in the boundary layer

M. Combe et al.

Title Page

Abstract

Introduction

Conclusions

References

Tables

Figures



Back

Close

Full Screen / Esc

Printer-friendly Version

Interactive Discussion

et al., 2004; Chen and Dudhia, 2001; Jacobs and de Bruin, 1997). Studies involving two-way coupled models like Santanello et al. (2013); Tao et al. (2013); Chen and Xie (2011) and Kohler et al. (2010) have stressed the importance of slowly evolving surface forcings such as soil moisture, vegetation cover and LAI, which drive the surface exchange and strongly impact atmospheric properties like boundary-layer height. Placing special emphasis on the upper atmosphere conditions, van Heerwaarden et al. (2009) and Ek and Holtslag (2004) have shown the impact of the ABL-top moisture inversion and the tropospheric temperature lapse rate, on the surface fluxes, relative humidity at top of the ABL and the boundary-layer cloud formation. With our sensitivity analysis, we moreover emphasize the importance of another large-scale atmospheric forcing, high subsidence, which affects surface fluxes and changes boundary-layer properties like temperature, moisture and CO<sub>2</sub> mole fraction.

We note that the satisfactory performance of coupled models depends on the correct initialization of the model for key surface and upper-atmospheric variables, as suggested by Sabater et al. (2008). In our study, the MXL-A-g<sub>s</sub> model profits especially from the explicit initialization of soil moisture. In that respect, we regard data assimilation of soil moisture values, as done e.g. in Boussetta et al. (2013); Hong et al. (2009) and de Wit and Van Diepen (2007), as a promising solution. Data assimilation of LAI, as done by Huang et al. (2013); Zhao et al. (2013); Sus et al. (2010) and Jégo et al. (2012), could also help transform our diurnal land-surface scheme A-g<sub>s</sub> into a capable seasonal surface scheme, as previously done within ISBA-A-g<sub>s</sub> (Barbu et al., 2011). Albergel et al. (2010) and Ines et al. (2013) suggest joint assimilation of LAI and soil moisture yields the best results. As an alternative, the MXL-A-g<sub>s</sub> model could also benefit from a satisfactory crop phenology module to interactively calculate LAI, like GECROS, as a replacement of LAI data assimilation (e.g. Lokupitiya et al., 2009).

One very important determinant of the impact of soil moisture availability on vegetation growth is the water-stress response of a model. The two models used here had a strongly differing response, with GECROS only reducing its conductivity, and hence evaporation, close to wilting point, and A-g<sub>s</sub> linearly decreasing stomatal conductance

from field capacity to wilting point. These are similar water-stress responses as for respectively the CLM3.5 and JULES models shown in Powell et al. (2013). We have confirmed that these differences in water-stress functions are responsible for the over-estimation of latent heat by MXL-GECROS compared to MXL-A-g<sub>s</sub>. We conclude, in agreement with Eitzinger et al. (2013) and Powell et al. (2013), that these differences in water-stress implementation could lead to significant differences in simulated crop yield.

Interpretations of observed CO<sub>2</sub> mole fractions in the ABL often focus on the role of NEE, typically a large contributor to the atmospheric CO<sub>2</sub> budget (Tolk et al., 2009). While we agree NEE is a key component, we recommend using a fully coupled land-atmosphere framework as we confirm that the land-induced boundary-layer growth has an important impact on the diurnal atmospheric CO<sub>2</sub> budget, due to both volume dilution and CO<sub>2</sub> entrainment (Canut et al., 2012; Mcgrath-Spangler and Denning, 2010; van Heerwaarden et al., 2009; Casso-Torralba et al., 2008; Vilà-Guerau De Arellano et al., 2004).

It is interesting to compare our study of the diurnal-scale controls on atmospheric CO<sub>2</sub> to the observation-based work of Williams et al. (2011). They showed that on longer time periods than the typical ten-day synoptic scale, NEE and large-scale air masses motions are the most important contributions to the atmospheric CO<sub>2</sub> mole fractions observed in the ABL. Errors in the modelled day-to-day variations of ABL growth rates and associated entrainment could thus be neglected when interpreting weekly to seasonally averaged CO<sub>2</sub> time series, which would support uncoupled frameworks where NEE is given as a boundary condition to CO<sub>2</sub> transport models. Nevertheless, such a use of uncoupled modelling frameworks is only justifiable if diurnal boundary-layer processes cannot yield significant changes in NEE. As shown by Eitzinger et al. (2013); Sánchez et al. (2014) and by our seasonal yield analysis in Sect. 3.1, wheat and maize have sensitive periods of less than 2 weeks (e.g. crop germination, anthesis/flowering, ripening) which can generate important differences in crop yield (i.e. NPP) if heat or water stress is applied. Using a diurnal scale coupled

## BGD

11, 5275–5325, 2014

### Two perspectives on coupled exchange in the boundary layer

M. Combe et al.

Title Page

Abstract

Introduction

Conclusions

References

Tables

Figures

⏪

⏩

◀

▶

Back

Close

Full Screen / Esc

Printer-friendly Version

Interactive Discussion



framework could thus be relevant for determining the surface fluxes of heat, water and CO<sub>2</sub> during those specific periods of crop development. A further investigation of the interactions identified in this work, focusing on the synoptic and seasonal time scales described in Williams et al. (2011), is therefore planned as a follow-up study.

## 5 Conclusions

We investigate the performance of an atmospheric mixed-layer model coupled to two different land-surface schemes, a atmospheric-oriented vs. a carbon storage-oriented model, to simulate the interactions of a maize cropland with the atmosphere. In order to explore the performance of both couplings, we compare them against a comprehensive set of observations of crop growth, surface exchange and boundary-layer variables for a maize field in the Netherlands on a clear, convective day. Because the applied models and observations cover the same spatial scale, it allows us to draw conclusions about the processes at work in the diurnal crop-atmosphere system.

To answer our first research question, we demonstrate that the diurnal cycles of heat, water and CO<sub>2</sub> are joined in a coupled system: through (a) the canopy stomatal control on CO<sub>2</sub> exchange and transpiration, which in turn determines the amount of sensible heat flux in the surface energy balance, and (b) the large-scale conditions at the top of the boundary layer, which control the diurnal boundary-layer development and thus the entrainment and volume dilution of heat, water and CO<sub>2</sub>. Our findings show these surface and upper atmospheric controls are of equivalent importance on a diurnal scale for the atmospheric CO<sub>2</sub> budget.

In response to our second research question, we show that neither of our models is able to simultaneously reproduce the diurnal heat, water and CO<sub>2</sub> surface fluxes. MXL-A-g<sub>s</sub> simulates the crop-interactions more satisfactorily overall, but it underestimates NEE. Its performance strongly depends on the sensitivity of the water-stress function to soil moisture, which is different in the two models. As a result, we recommend using meteorological-oriented (surface exchange) models, such as MXL-A-g<sub>s</sub>,

**BGD**

11, 5275–5325, 2014

## Two perspectives on coupled exchange in the boundary layer

M. Combe et al.

Title Page

Abstract

Introduction

Conclusions

References

Tables

Figures

◀

▶

◀

▶

Back

Close

Full Screen / Esc

Printer-friendly Version

Interactive Discussion



## Two perspectives on coupled exchange in the boundary layer

M. Combe et al.

Title Page

Abstract

Introduction

Conclusions

References

Tables

Figures

◀

▶

◀

▶

Back

Close

Full Screen / Esc

Printer-friendly Version

Interactive Discussion



for simulations of the diurnal crop-atmosphere interactions, as long as the crop is not nitrogen-stressed. However, to simulate longer periods of crop-atmosphere interactions, we recommend to adopt a cut-and-paste strategy to use the distinct advantages of both meteorological-oriented land-surface models (sound surface energy balance) and carbon storage-oriented vegetation models (crop phenology, nitrogen stress implementation and prognostic carbon pools). A first step towards this goal, in our case, would be to adapt the A-g<sub>s</sub> for seasonal simulations, using a satisfactory crop phenology module.

Finally, we advocate the use of complete sets of observations, including not only soil, vegetation, and lower atmosphere, but also boundary layer and free troposphere, to evaluate the performance of coupled land-atmosphere models. These prove of utmost importance for the validation of the modelled interactions.

*Acknowledgements.* This research was funded by the Netherlands Organisation for Scientific Research (NWO) through the VIDI grant number 864.08.012. The authors acknowledge Xinyou Yin (Wageningen University) and Kees Rappoldt (EcoCurves BV) for their expert help with the GECROS model. We also thank Henk Klein Baltink (KNMI) and Fred Bosveld (KNMI) for providing the Cabauw data, Eduardo Barbaro (Wageningen University) for his scientific opinion on the radiation formulation, and Denica Bozhinova (Wageningen University) for her help with programming a part of the analysis code.

## References

- Ahmadov, R., Gerbig, C., Kretschmer, R., Koerner, S., Neininger, B., Dolman, A. J., and Sarfat, C.: Mesoscale covariance of transport and CO<sub>2</sub> fluxes: Evidence from observations and simulations using the WRF-VPRM coupled atmosphere-biosphere model, *J. Geophys. Res.*, 112, D22107, doi:10.1029/2007JD008552, 2007. 5278
- Albergel, C., Calvet, J.-C., Mahfouf, J.-F., Rüdiger, C., Barbu, A. L., Lafont, S., Roujean, J.-L., Walker, J. P., Crapeau, M., and Wigneron, J.-P.: Monitoring of water and carbon fluxes using a land data assimilation system: a case study for southwestern France, *Hydrol. Earth Syst. Sci.*, 14, 1109–1124, doi:10.5194/hess-14-1109-2010, 2010. 5299

## Two perspectives on coupled exchange in the boundary layer

M. Combe et al.

Title Page

Abstract

Introduction

Conclusions

References

Tables

Figures

◀

▶

◀

▶

Back

Close

Full Screen / Esc

Printer-friendly Version

Interactive Discussion



- Aubinet, M., Vesala, T., and Papale, D. (Eds.): Eddy Covariance: A Practical Guide to Measurement and Data Analysis, Springer, Dordrecht, the Netherlands, 2012. 5281, 5318, 5320
- Ball, J. T.: An analysis of stomatal conductance, Ph.D. thesis, Stanford University, Stanford, CA, 1988. 5277
- 5 Barbu, A. L., Calvet, J.-C., Mahfouf, J.-F., Albergel, C., and Lafont, S.: Assimilation of Soil Wetness Index and Leaf Area Index into the ISBA-A-gs land surface model: grassland case study, *Biogeosciences*, 8, 1971–1986, doi:10.5194/bg-8-1971-2011, 2011. 5299
- Bert, F. E., Laciana, C. E., Podestá, G. P., Satorre, E. H., and Menéndez, A. N.: Sensitivity of CERES-Maize simulated yields to uncertainty in soil properties and daily solar radiation, *Agr. Syst.*, 94, 141–150, doi:10.1016/j.agsy.2006.08.003, 2007. 5278
- 10 Betts, A. K.: Non-precipitating cumulus convection and its parameterization, *Q. J. Roy. Meteor. Soc.*, 99, 178–196, doi:10.1002/qj.49709941915, 1973. 5282
- Betts, A. K.: Understanding hydrometeorology using global models, *B. Am. Meteorol. Soc.*, 85, 1673–1688, 2004. 5289
- 15 Betts, R. A.: Integrated approaches to climate-crop modelling: needs and challenges, *Philos. T. Roy. Soc. B*, 360, 2049–2065, 2005. 5279, 5280
- Bonan, G. B.: Forests and climate change: forcings, feedbacks, and the climate benefits of forests, *Science*, 320, 1444–1449, 2008. 5277
- Boussetta, S., Balsamo, G., Beljaars, A., Panareda, A. A., Calvet, J. C., Jacobs, C., Van Den Hurk, B., Viterbo, P., Lafont, S., Dutra, E., Jarlan, L., Balzarolo, M., Papale, D., and Van Der Werf, G.: Natural land carbon dioxide exchanges in the ECMWF integrated forecasting system: implementation and offline validation, *J. Geophys. Res.-Atmos.*, 118, 5923–5946, 2013. 5298, 5299
- 20 Brienens, R., Wanek, W., and Hietz, P.: Stable carbon isotopes in tree rings indicate improved water use efficiency and drought responses of a tropical dry forest tree species, *Trees*, 25, 103–113, doi:10.1007/s00468-010-0474-1, 2011. 5277
- Canut, G., Couvreux, F., Lothon, M., Pino, D., and Saïd, F.: Observations and large-eddy simulations of entrainment in the sheared sahelian boundary layer, *Bound.-Lay. Meteorol.*, 142, 79–101, 2012. 5300
- 30 Carson, D. J.: The development of a dry inversion-capped convectively unstable boundary layer, *Q. J. Roy. Meteor. Soc.*, 99, 450–467, doi:10.1002/qj.49709942105, 1973. 5282
- Casso-Torralba, P., Vilà-Guerau de Arellano, J., Bosveld, F., Soler, M. R., Vermeulen, A., Werner, C., and Moors, E.: Diurnal and vertical variability of the sensible heat and car-

## Two perspectives on coupled exchange in the boundary layer

M. Combe et al.

Title Page

Abstract

Introduction

Conclusions

References

Tables

Figures

◀

▶

◀

▶

Back

Close

Full Screen / Esc

Printer-friendly Version

Interactive Discussion



bon dioxide budgets in the atmospheric surface layer, *J. Geophys. Res.*, 113, D12119, doi:10.1029/2007JD009583, 2008. 5294, 5300

Challinor, A. J., Ewert, F., Arnold, S., Simelton, E., and Fraser, E.: Crops and climate change: progress, trends, and challenges in simulating impacts and informing adaptation, *J. Exp. Bot.*, 60, 2775–2789, 2009. 5279

Chen, F. and Dudhia, J.: Coupling an advanced land surface–hydrology model with the Penn State–NCAR MM5 modeling system. Part II: Preliminary model validation, *Mon. Weather Rev.*, 129, 587–604, 2001. 5299

Chen, F. and Xie, Z.: Effects of crop growth and development on regional climate: a case study over East Asian monsoon area, *Clim. Dynam.*, 38, 2291–2305, 2011. 5299

Ciais, P., Wattenbach, M., Vuichard, N., Smith, P., Piao, S. L., Don, A., Luysaert, S., Janssens, I. A., Bondeau, A., Dechow, R., Leip, A., Smith, P. C., Beer, C., van der Werf, G., Gervois, S., van Oost, K., Tomelleri, E., Freibauer, A., and Schulze, E. D.: The European carbon balance. Part 2: Croplands, *Glob. Change Biol.*, 16, 1409–1428, 2010. 5279

Collatz, G. J., Ball, J. T., Grivet, C., and Berry, J. A.: Physiological and environmental regulation of stomatal conductance, photosynthesis and transpiration: a model that includes a laminar boundary layer, *Agr. Forest Meteorol.*, 54, 107–136, 1991. 5277

Corbin, K. D., Denning, A. S., Lokupitiya, E. Y., Schuh, A. E., Miles, N. L., Davis, K. J., Richardson, S., and Baker, I. T.: Assessing the impact of crops on regional CO<sub>2</sub> fluxes and atmospheric concentrations, *Tellus B*, 62, 521–532, doi:10.1111/j.1600-0889.2010.00485.x, 2010. 5278, 5298

Cowan, I. R.: Stomatal behaviour and environment, *Adv. Bot. Res.*, 4, 117–228, 1978. 5277

Cox, P. M., Pearson, D., Booth, B. B., Friedlingstein, P., Huntingford, C., Jones, C. D., and Luke, C. M.: Sensitivity of tropical carbon to climate change constrained by carbon dioxide variability, *Nature*, 494, 341–344, doi:10.1038/nature11882, 2013. 5277, 5278

Daly, E., Porporato, A., and Rodriguez-Iturbe, I.: Coupled dynamics of photosynthesis, transpiration, and soil water balance. Part II: Stochastic analysis and ecohydrological significance, *J. Hydrometeorol.*, 5, 559–566, 2004. 5289

Davin, E. L., Stöckli, R., Jaeger, E. B., Levis, S., and Seneviratne, S. I.: COSMO-CLM2: A new version of the COSMO-CLM model coupled to the Community Land Model, *Clim. Dynam.*, 37, 1889–1907, 2011. 5298

## Two perspectives on coupled exchange in the boundary layer

M. Combe et al.

Title Page

Abstract

Introduction

Conclusions

References

Tables

Figures

◀

▶

◀

▶

Back

Close

Full Screen / Esc

Printer-friendly Version

Interactive Discussion



- de Bruin, H. A. R. and Holtslag, A. A. M.: A simple parameterization of the surface fluxes of sensible and latent-heat during daytime compared with the Penman–Monteith concept, *J. Appl. Meteorol.*, 21, 1610–1621, 1982. 5285
- De Pury, D. G. G. and Farquhar, G. D.: Simple scaling of photosynthesis from leaves to canopies without the errors of big-leaf models, *Plant Cell Environ.*, 20, 537–557, 1997. 5283
- de Wit, A. J. W. and Van Diepen, C. A.: Crop model data assimilation with the Ensemble Kalman filter for improving regional crop yield forecasts, *Agr. Forest Meteorol.*, 146, 38–56, 2007. 5298, 5299
- Dirmeyer, P. A., Koster, R. D., and Guo, Z.: Do global models properly represent the feedback between land and atmosphere?, *J. Hydrometeorol.*, 7, 1177–1198, 2006. 5298
- Eitzinger, J., Formayer, H., Thaler, S., Trnka, M., Zdenek, Z., and Alexandrov, V.: Aspects on results and uncertainties of climate change impact simulation studies for agricultural crop production in Europe, *Bodenkultur*, 59, 131–147, 2008. 5280
- Eitzinger, J., Thaler, S., Schmid, E., Strauss, F., Ferrise, R., Moriondo, M., Bindi, M., Palosuo, T., Rötter, R., Kersebaum, K. C., Olesen, J. E., Patil, R. H., Şaylan, L., Çaldağ, B., and Çaylak, O.: Sensitivities of crop models to extreme weather conditions during flowering period demonstrated for maize and winter wheat in Austria, *J. Agr. Sci.*, 151, 813–835, 2013. 5300
- Ek, M. B. and Holtslag, A. A. M.: Influence of soil moisture on boundary layer cloud development, *J. Hydrometeorol.*, 5, 86–99, 2004. 5299
- FAOSTAT 2011 land-use statistics: The land-use resources sub-domain covers land area, temporary crops area and permanent crops area, FAOSTAT online database, available at: <http://faostat3.fao.org/faostat-gateway/go/to/download/R/RL/E> (last access: 3 March 2014), 2014. 5279
- Farquhar, G. D., O’leary, M. H., and Berry, J. A.: On the relationship between carbon isotope discrimination and the intercellular carbon dioxide concentration in leaves, *Aust. J. of Plant Physiol.*, 9, 121–137, 1982. 5277
- Foken, T., Mauder, M., Liebethal, C., Wimmer, F., Beyrich, F., Leps, J. P., Raasch, S., De Bruin, H. A. R., Meijninger, W. M. L., and Bange, J.: Energy balance closure for the LITFASS-2003 experiment, *Theor. Appl. Climatol.*, 101, 149–160, 2010. 5281
- Friedlingstein, P., Cox, P., Betts, R., Bopp, L., Von Bloh, W., Brovkin, V., Cadule, P., Doney, S., Eby, M., Fung, I., Bala, G., John, J., Jones, C., Joos, F., Kato, T., Kawamiya, M., Knorr, W., Lindsay, K., Matthews, H. D., Raddatz, T., Rayner, P., Reick, C., Roeckner, E., Schnit-

## Two perspectives on coupled exchange in the boundary layer

M. Combe et al.

[Title Page](#)

[Abstract](#)

[Introduction](#)

[Conclusions](#)

[References](#)

[Tables](#)

[Figures](#)

[⏪](#)

[⏩](#)

[◀](#)

[▶](#)

[Back](#)

[Close](#)

[Full Screen / Esc](#)

[Printer-friendly Version](#)

[Interactive Discussion](#)



zler, K. G., Schnur, R., Strassmann, K., Weaver, A. J., Yoshikawa, C., and Zeng, N.: Climate–carbon cycle feedback analysis: results from the C<sup>4</sup>MIP model intercomparison, *J. Climate*, 19, 3337–3353, doi:10.1175/JCLI3800.1, 2006. 5278

Gervois, S., Ciais, P., de Noblet-Ducoudré, N., Brisson, N., Vuichard, N., and Viovy, N.: Carbon and water balance of European croplands throughout the 20th century, *Global Biogeochem. Cy.*, 22, GB2022, doi:10.1029/2007GB003018, 2008. 5279

Hong, S., Lakshmi, V., Small, E. E., Chen, F., Tewari, M., and Manning, K. W.: Effects of vegetation and soil moisture on the simulated land surface processes from the coupled WRF/Noah model, *J. Geophys. Res.-Atmos.*, 114, D18118, doi:10.1029/2008JD011249, 2009. 5298, 5299

Huang, Y., Zhu, Y., Li, W. L., Cao, W. X., and Tian, Y. C.: Assimilating remotely sensed information with the wheatgrow model based on the ensemble square root filter for improving regional wheat yield forecasts, *Plant Prod. Sci.*, 16, 352–364, 2013. 5299

Ines, A. V. M., Das, N. N., Hansen, J. W., and Njoku, E. G.: Assimilation of remotely sensed soil moisture and vegetation with a crop simulation model for maize yield prediction, *Remote Sens. Environ.*, 138, 149–164, 2013. 5299

Jacobs, C. M. J. and de Bruin, H. A. R.: Predicting regional transpiration at elevated atmospheric CO<sub>2</sub>: influence of the PBL–vegetation interaction, *J. Appl. Meteorol.*, 36, 1663–1675, 1997. 5299

Jacobs, C. M. J., van den Hurk, B. M. M., and de Bruin, H. A. R.: Stomatal behaviour and photosynthetic rate of unstressed grapevines in semi-arid conditions, *Agr. Forest Meteorol.*, 80, 111–134, 1996. 5277

Jacobs, C. M. J., Jacobs, A. F. G., Bosveld, F. C., Hendriks, D. M. D., Hensen, A., Kroon, P. S., Moors, E. J., Nol, L., Schrier-Uijl, A., and Veenendaal, E. M.: Variability of annual CO<sub>2</sub> exchange from Dutch grasslands, *Biogeosciences*, 4, 803–816, doi:10.5194/bg-4-803-2007, 2007. 5288

Jans, W. W. P., Jacobs, C. M. J., Kruijt, B., Elbers, J. A., Barendse, S., and Moors, E. J.: Carbon exchange of a maize (*Zea mays* L.) crop: influence of phenology, *Agr. Ecosyst. Environ.*, 139, 316–324, 2010. 5279, 5281, 5287, 5288

Jarvis, P. G.: The Interpretation of the Variations in Leaf Water Potential and Stomatal Conductance Found in Canopies in the Field, *Philos. T. Roy. Soc. B*, 273, 593–610, 1976. 5277

## Two perspectives on coupled exchange in the boundary layer

M. Combe et al.

Title Page

Abstract

Introduction

Conclusions

References

Tables

Figures

◀

▶

◀

▶

Back

Close

Full Screen / Esc

Printer-friendly Version

Interactive Discussion



Jégo, G., Pattey, E., and Liu, J.: Using Leaf Area Index, retrieved from optical imagery, in the STICS crop model for predicting yield and biomass of field crops, *Field Crop. Res.*, 131, 63–74, 2012. 5299

Keenan, T. F., Hollinger, D. Y., Bohrer, G., Dragoni, D., Munger, J. W., Schmid, H. P., and Richardson, A. D.: Increase in forest water-use efficiency as atmospheric carbon dioxide concentrations rise, *Nature*, 499, 324–327, 2013. 5277

Kohler, M., Kalthoff, N., and Kottmeier, C.: The impact of soil moisture modifications on CBL characteristics in West Africa: a case-study from the AMMA campaign, *Q. J. Roy. Meteor. Soc.*, 136, 442–455, 2010. 5299

Krinner, G., Viovy, N., De Noblet-Ducoudré, N., Ogée, J., Polcher, J., Friedlingstein, P., Ciais, P., Sitch, S., and Prentice, I. C.: A dynamic global vegetation model for studies of the coupled atmosphere-biosphere system, *Global Biogeochem. Cy.*, 19, 1–33, 2005. 5279

Lehuger, S., Gabrielle, B., Cellier, P., Loubet, B., Roche, R., Béziat, P., Ceschia, E., and Wattenbach, M.: Predicting the net carbon exchanges of crop rotations in Europe with an agro-ecosystem model, *Agr. Ecosyst. Environ.*, 139, 384–395, 2010. 5279

Leuning, R., Kelliher, F. M., Pury, D. G. G., and Schulze, E. D.: Leaf nitrogen, photosynthesis, conductance and transpiration: scaling from leaves to canopies, *Plant Cell Environ.*, 18, 1183–1200, 1995. 5277

Lilly, D. K.: Models of cloud-topped mixed layers under a strong inversion, *Q. J. Roy. Meteor. Soc.*, 94, 292–309, 1968. 5282

Liu, Y., Gupta, H. V., Sorooshian, S., Bastidas, L. A., and Shuttleworth, W. J.: Exploring parameter sensitivities of the land surface using a locally coupled land-atmosphere model, *J. Geophys. Res.-Atmos.*, 109, D21101, doi:10.1029/2004JD004730, 2004. 5298

Lobell, D. B., Schlenker, W., and Costa-Roberts, J.: Climate trends and global crop production since 1980, *Science*, 333, 616–620, 2011. 5277

Lokupitiya, E., Denning, S., Paustian, K., Baker, I., Schaefer, K., Verma, S., Meyers, T., Bernacchi, C. J., Suyker, A., and Fischer, M.: Incorporation of crop phenology in Simple Biosphere Model (SiBcrop) to improve land-atmosphere carbon exchanges from croplands, *Biogeosciences*, 6, 969–986, doi:10.5194/bg-6-969-2009, 2009. 5299

Mcgrath-Spangler, E. L. and Denning, A. S.: Impact of entrainment from overshooting thermals on land-atmosphere interactions during summer 1999, *Tellus B*, 62, 441–454, 2010. 5278, 5300

## Two perspectives on coupled exchange in the boundary layer

M. Combe et al.

Title Page

Abstract

Introduction

Conclusions

References

Tables

Figures

◀

▶

◀

▶

Back

Close

Full Screen / Esc

Printer-friendly Version

Interactive Discussion



- Meyers, T. P. and Hollinger, S. E.: An assessment of storage terms in the surface energy balance of maize and soybean, *Agr. Forest Meteorol.*, 125, 105–115, 2004. 5281
- Moreira, D. S., Freitas, S. R., Bonatti, J. P., Mercado, L. M., Rosário, N. M. É., Longo, K. M., Miller, J. B., Gloor, M., and Gatti, L. V.: Coupling between the JULES land-surface scheme and the CCATT-BRAMS atmospheric chemistry model (JULES-CCATT-BRAMS1.0): applications to numerical weather forecasting and the CO<sub>2</sub> budget in South America, *Geosci. Model Dev.*, 6, 1243–1259, doi:10.5194/gmd-6-1243-2013, 2013. 5298
- Pino, D., Vilà-Guerau de Arellano, J., Peters, W., Schröter, J., van Heerwaarden, C. C., and Krol, M. C.: A conceptual framework to quantify the influence of convective boundary layer development on carbon dioxide mixing ratios, *Atmos. Chem. Phys.*, 12, 2969–2985, doi:10.5194/acp-12-2969-2012, 2012. 5298
- Powell, T. L., Galbraith, D. R., Christoffersen, B. O., Harper, A., Imbuzeiro, H. M. A., Rowland, L., Almeida, S., Brando, P. M., da Costa, A. C. L., Costa, M. H., Levine, N. M., Malhi, Y., Saleska, S. R., Sotta, E., Williams, M., Meir, P., and Moorcroft, P. R.: Confronting model predictions of carbon fluxes with measurements of Amazon forests subjected to experimental drought, *The New Phytol.*, 200, 350–365, 2013. 5300
- Ronda, R. J., De Bruin, H., and Holtslag, A.: Representation of the canopy conductance in modeling the surface energy budget for low vegetation, *J. Appl. Meteorol.*, 40, 1431–1444, 2001. 5279, 5285, 5287
- Sabater, J. M., Rüdiger, C., Calvet, J. C., Fritz, N., Jarlan, L., and Kerr, Y.: Joint assimilation of surface soil moisture and LAI observations into a land surface model, *Agr. Forest Meteorol.*, 148, 1362–1373, 2008. 5299
- Sánchez, B., Rasmussen, A., and Porter, J. R.: Temperatures and the growth and development of maize and rice: a review, *Glob. Change Biol.*, 20, 408–417, 2014. 5300
- Santanello Jr., J. A., Peters-Lidard, C. D., Kennedy, A., and Kumar, S. V.: Diagnosing the nature of land–atmosphere coupling: a case study of dry/wet extremes in the U. S. Southern Great Plains, *J. Hydrometeorol.*, 14, 3–24, 2013. 5278, 5298, 5299
- Schuh, A. E., Denning, A. S., Corbin, K. D., Baker, I. T., Uliasz, M., Parazoo, N., Andrews, A. E., and Worthy, D. E. J.: A regional high-resolution carbon flux inversion of North America for 2004, *Biogeosciences*, 7, 1625–1644, doi:10.5194/bg-7-1625-2010, 2010. 5298
- Silva, L. C. R. and Horwath, W. R.: Explaining global increases in water use efficiency: why have we overestimated responses to rising atmospheric CO<sub>2</sub> in natural forest ecosystems?, *PLoS ONE*, 8, e53089, doi:10.1371/journal.pone.0053089, 2013. 5277

## Two perspectives on coupled exchange in the boundary layer

M. Combe et al.

Title Page

Abstract

Introduction

Conclusions

References

Tables

Figures



Back

Close

Full Screen / Esc

Printer-friendly Version

Interactive Discussion

- Sinclair, T. S. and de Wit, C. T.: Photosynthate and nitrogen requirements for seed production by various crops, *Science*, 189, 565–567, 1975. 5286, 5316
- Sitch, S., Smith, B., Prentice, I. C., Arneth, A., Bondeau, A., Cramer, W., Kaplan, J. O., Levis, S., Lucht, W., and Sykes, M. T.: Evaluation of ecosystem dynamics, plant geography and terrestrial carbon cycling in the LPJ dynamic global vegetation model, *Glob. Change Biol.*, 9, 161–185, 2003. 5278, 5279
- Sitch, S., Huntingford, C., Gedney, N., Levy, P. E., Lomas, M., Piao, S. L., Betts, R., Ciais, P., Cox, P., Friedlingstein, P., Jones, C. D., Prentice, I. C., and Woodward, F. I.: Evaluation of the terrestrial carbon cycle, future plant geography and climate–carbon cycle feedbacks using five Dynamic Global Vegetation Models (DGVMs), *Glob. Change Biol.*, 14, 2015–2039, doi:10.1111/j.1365-2486.2008.01626.x, 2008. 5277
- Smallman, T. L., Moncrieff, J. B., and Williams, M.: WRFv3.2-SPA v2: development and validation of a coupled ecosystem–atmosphere model, scaling from surface fluxes of CO<sub>2</sub> and energy to atmospheric profiles, *Geosci. Model Dev.*, 6, 1079–1093, doi:10.5194/gmd-6-1079-2013, 2013. 5298
- Smith, P. C., De Noblet-Ducoudré, N., Ciais, P., Peylin, P., Viovy, N., Meurdesoif, Y., and Bondeau, A.: European-wide simulations of croplands using an improved terrestrial biosphere model: Phenology and productivity, *J. Geophys. Res.*, 115, G01014, doi:10.1029/2008JG000800, 2010. 5278
- Subin, Z. M., Riley, W. J., Jin, J., Christianson, D. S., Torn, M. S., and Kueppers, L. M.: Ecosystem feedbacks to climate change in California: development, testing, and analysis using a coupled regional atmosphere and land surface model (WRF3-CLM3.5), *B. Am. Meteorol. Soc.*, 15, 1–38, 2011. 5298
- Sus, O., Williams, M., Bernhofer, C., Béziat, P., Buchmann, N., Ceschia, E., Doherty, R., Eugster, W., Grünwald, T., Kutsch, W., Smith, P., and Wattenbach, M.: A linked carbon cycle and crop developmental model: Description and evaluation against measurements of carbon fluxes and carbon stocks at several European agricultural sites, *Agr. Ecosyst. Environ.*, 139, 402–418, 2010. 5299
- Tao, Z., Santanello, J. A., Chin, M., Zhou, S., Tan, Q., Kemp, E. M., and Peters-Lidard, C. D.: Effect of land cover on atmospheric processes and air quality over the continental United States – a NASA Unified WRF (NU-WRF) model study, *Atmos. Chem. Phys.*, 13, 6207–6226, doi:10.5194/acp-13-6207-2013, 2013. 5299

**Two perspectives on coupled exchange in the boundary layer**

M. Combe et al.

[Title Page](#)[Abstract](#)[Introduction](#)[Conclusions](#)[References](#)[Tables](#)[Figures](#)[◀](#)[▶](#)[◀](#)[▶](#)[Back](#)[Close](#)[Full Screen / Esc](#)[Printer-friendly Version](#)[Interactive Discussion](#)

- Tennekes, H.: A model for the dynamics of the inversion above a convective boundary layer, *J. Atmos. Sci.*, 30, 558–567, 1973. 5282
- Teuling, A. J., Seneviratne, S. I., Stöckli, R., Reichstein, M., Moors, E., Ciais, P., Luysaert, S., van den Hurk, B., Ammann, C., Bernhofer, C., Dellwik, E., Gianelle, D., Gielen, B., Grünwald, T., Klumpp, K., Montagnani, L., Moureaux, C., Sottocornola, M., and Wohlfhart, G.: Contrasting response of European forest and grassland energy exchange to heatwaves, *Nat. Geosci.*, 3, 722–727, doi:10.1038/ngeo950, 2010. 5277
- Tolk, L. F., Peters, W., Meesters, A. G. C. A., Groenendijk, M., Vermeulen, A. T., Steeneveld, G. J., and Dolman, A. J.: Modelling regional scale surface fluxes, meteorology and CO<sub>2</sub> mixing ratios for the Cabauw tower in the Netherlands, *Biogeosciences*, 6, 2265–2280, doi:10.5194/bg-6-2265-2009, 2009. 5278, 5298, 5300
- Twine, T. E., Kustas, W. P., Norman, J. M., Cook, D. R., Houser, P. R., Meyers, T. P., Prueger, J. H., Starks, P. J., and Wesely, M. L.: Correcting eddy-covariance flux underestimates over a grassland, *Agr. Forest Meteorol.*, 103, 279–300, 2000. 5282
- van Heerwaarden, C. C., Vilà-Guerau de Arellano, J., Moene, A. F., and Holtslag, A. A. M.: Interactions between dry-air entrainment, surface evaporation and convective boundary-layer development, *Q. J. Roy. Meteor. Soc.*, 135, 1277–1291, 2009. 5278, 5294, 5299, 5300
- van Heerwaarden, C. C., Vilà-Guerau De Arellano, J., and Teuling, A. J.: Land-atmosphere coupling explains the link between pan evaporation and actual evapotranspiration trends in a changing climate, *Geophys. Res. Lett.*, 37, L21401, doi:10.1029/2010GL045374, 2010. 5298
- Vilà-Guerau De Arellano, J., Gioli, B., Miglietta, F., Jonker, H. J. J., Baltink, H. K., Hutjes, R. W. A., and Holtslag, A. A. M.: Entrainment process of carbon dioxide in the atmospheric boundary layer, *J. Geophys. Res.-Atmos.*, 109, D18110, doi:10.1029/2004JD004725, 2004. 5300
- Vilà-Guerau de Arellano, J., van den Dries, K., and Pino, D.: On inferring isoprene emission surface flux from atmospheric boundary layer concentration measurements, *Atmos. Chem. Phys.*, 9, 3629–3640, doi:10.5194/acp-9-3629-2009, 2009. 5282
- Vilà-Guerau de Arellano, J., van Heerwaarden, C. C., and Lelieveld, J.: Modelled suppression of boundary-layer clouds by plants in a CO<sub>2</sub>-rich atmosphere, *Nat. Geosci.*, 5, 1–4, 2012. 5277, 5278, 5298

**Two perspectives on coupled exchange in the boundary layer**

M. Combe et al.

[Title Page](#)[Abstract](#)[Introduction](#)[Conclusions](#)[References](#)[Tables](#)[Figures](#)[⏪](#)[⏩](#)[◀](#)[▶](#)[Back](#)[Close](#)[Full Screen / Esc](#)[Printer-friendly Version](#)[Interactive Discussion](#)

- Williams, I. N., Riley, W. J., Torn, M. S., Berry, J. A., and Biraud, S. C.: Using boundary layer equilibrium to reduce uncertainties in transport models and CO<sub>2</sub> flux inversions, *Atmos. Chem. Phys.*, 11, 9631–9641, doi:10.5194/acp-11-9631-2011, 2011. 5300, 5301
- 5 Wramneby, A., Smith, B., and Samuelsson, P.: Hot spots of vegetation-climate feedbacks under future greenhouse forcing in Europe, *J. Geophys. Res.*, 115, D21119, doi:10.1029/2010JD014307, 2010. 5298
- Yin, X. and van Laar, H. H.: *Crop Systems Dynamics: An Ecophysiological Simulation Model for Genotype-by-Environment Interactions*, Wageningen Academic Publishers, Wageningen, the Netherlands, 2005. 5279, 5283, 5286, 5290, 5316
- 10 Zhao, W. and Qualls, R. J.: Modeling of long-wave and net radiation energy distribution within a homogeneous plant canopy via multiple scattering processes, *Water Resour. Res.*, 42, W08436, doi:10.1029/2005WR004581, 2006. 5284
- 15 Zhao, Y., Chen, S., and Shen, S.: Assimilating remote sensing information with crop model using Ensemble Kalman Filter for improving LAI monitoring and yield estimation, *Ecol. Model.*, 270, 30–42, 2013. 5299

## Two perspectives on coupled exchange in the boundary layer

M. Combe et al.

Title Page

Abstract

Introduction

Conclusions

References

Tables

Figures

◀

▶

◀

▶

Back

Close

Full Screen / Esc

Printer-friendly Version

Interactive Discussion



**Table 1.** Seasonal statistics of the daily integrated Qnet, LE, SH and NEE from Fig. 2. Statistics are computed from sowing to maturity dates. We present the observed and modelled means and standard deviations, the root mean squared error (RMSE) between the model and the observations (in the same units as the mean) and the  $R^2$  between the model and the observations.

Variable [units]	Observed		Modelled		RMSE	$R^2$
	mean	stddev	mean	stddev		
Qnet [ $\text{MJm}^{-2}$ ]	8.9	3.7	8.1	4.4	1.4	0.95
LE [ $\text{MJm}^{-2}$ ]	5.9	2.5	5.5	3.5	1.8	0.75
SH [ $\text{MJm}^{-2}$ ]	1.7	1.3	1.8	1.7	1.1	0.59
NEE [ $\text{gCO}_2\text{m}^{-2}$ ]	-15.8	19.5	-19.1	28.8	16.0	0.74

## Two perspectives on coupled exchange in the boundary layer

M. Combe et al.

**Table 2.** Diurnal Integrals of Qnet, LE, SH and NEE from Fig. 4, calculated from 06:00 UTC to 18:00 UTC on the 4 August 2007.

	Qnet [MJm <sup>-2</sup> ]	LE [MJm <sup>-2</sup> ]	SH [MJm <sup>-2</sup> ]	NEE [gCO <sub>2</sub> m <sup>-2</sup> ]
Observations	15.6	9.3	4.4	-55.9
MXL-A-g <sub>s</sub>	14.6	8.7	5.1	-46.9
MXL-GECROS	17.0	12.2	3.1	-72.4

Title Page

Abstract

Introduction

Conclusions

References

Tables

Figures

⏪

⏩

◀

▶

Back

Close

Full Screen / Esc

Printer-friendly Version

Interactive Discussion



**Table A1.** MXL model initial conditions for the 4 August 2007.

variable	description and unit	value
latt	latitude [° N]	51.59
long	longitude [° E]	5.38
day	date [DOY]	216
cc	cloud cover [-]	0.225
$h_0$	initial boundary-layer height [m]	230.0
pressure	atmospheric pressure [hPa]	1022.0
$D$	large-scale divergence [ $s^{-1}$ ]	$7 \times 10^{-6}$
$\beta$	entrainment ratio [-]	0.2
$\theta_0$	initial potential temperature [K]	286.0
$\Delta\theta_0$	inital potential temperature jump [K]	5.0
$\gamma_\theta$	potential temperature lapse rate [ $Km^{-1}$ ]	$8 \times 10^{-3}$
adv $\theta$	initial heat advection flux [ $Ks^{-1}$ ]	$3 \times 10^{-4}$
adv $\theta$ tim	time of heat advection stop [UTC]	10:00
$q_0$	initial specific humidity [ $gkg^{-1}$ ]	8.5
$\Delta q_0$	initial specific humidity jump [ $gkg^{-1}$ ]	-1.0
$\gamma_q$	specific humidity lapse rate [ $gkg^{-1}m^{-1}$ ]	-0.0005
adv $q$	initial humidity advection flux [ $gkg^{-1}s^{-1}$ ]	$3.5 \times 10^{-4}$
adv $q$ tim	time of humidity advection stop [UTC]	07:30
$c_0$	initial CO <sub>2</sub> mole fraction [ppm]	422.0
$\Delta c_0$	initial CO <sub>2</sub> mole fraction jump [ppm]	-50.0
$\gamma_c$	CO <sub>2</sub> mole fraction lapse rate [ppb $m^{-1}$ ]	-10.0
$u_0$	initial mixed-layer u-wind speed [ $ms^{-1}$ ]	5.0
$u_g$	geostrophic u-wind speed [ $ms^{-1}$ ]	8.0
$\gamma_u$	free troposphere u-wind speed lapse rate [ $s^{-1}$ ]	0.0
$z_{0,m}$	roughness length for momentum [m]	0.15
$z_{0,h}$	roughness length for scalars [m]	0.015

## Two perspectives on coupled exchange in the boundary layer

M. Combe et al.

Title Page

Abstract

Introduction

Conclusions

References

Tables

Figures

◀

▶

◀

▶

Back

Close

Full Screen / Esc

Printer-friendly Version

Interactive Discussion



**Table A2.** A-g<sub>s</sub> model initial conditions for the 4 August 2007.

variable	description and unit	value
albedo	surface albedo [-]	0.198
LAI	Leaf Area Index [m <sup>2</sup> m <sup>-2</sup> ]	3.5
<i>f</i> <sub>veg</sub>	Vegetation fraction [-]	0.97
<i>r</i> <sub>s, min</sub>	Minimum resistance for transpiration [sm <sup>-1</sup> ]	180.0
<i>r</i> <sub>s, soil min</sub>	Minimum soil resistance [sm <sup>-1</sup> ]	50.0
Λ	Thermal diffusivity skin layer [Wm <sup>-2</sup> K <sup>-1</sup> ]	2.5
<i>g</i> <sub>D</sub>	VPD correction factor for rs [-]	0.
CG <sub>sat</sub>	Saturated heat soil conductivity [K m <sup>-2</sup> J <sup>-1</sup> ]	3.56 × 10 <sup>-6</sup>
<i>C</i> <sub>w</sub>	Constant water stress correction [-]	0.0016
<i>T</i> <sub>s</sub>	Initial surface temperature [K]	290.0
<i>T</i> <sub>soil</sub>	Temperature of top soil layer [K]	288.0
<i>T</i> <sub>2</sub>	Temperature of deeper soil layer [K]	289.0
<i>w</i> <sub>g</sub>	Water content top soil layer [cm <sup>3</sup> cm <sup>-3</sup> ]	0.11
<i>w</i> <sub>2</sub>	Water content deep soil layer [cm <sup>3</sup> cm <sup>-3</sup> ]	0.11
<i>w</i> <sub>sat</sub>	Saturation water content [cm <sup>3</sup> cm <sup>-3</sup> ]	0.36
<i>w</i> <sub>fc</sub>	Field capacity water content [cm <sup>3</sup> cm <sup>-3</sup> ]	0.15
<i>w</i> <sub>willt</sub>	Wilting point water content [cm <sup>3</sup> cm <sup>-3</sup> ]	0.06
<i>w</i> <sub>s, max</sub>	Upper reference value soil water [-]	0.55
<i>w</i> <sub>s, min</sub>	Lower reference value soil water [-]	0.005
<i>C</i> <sub>1, sat</sub>	Coefficient force term moisture [-]	0.132
<i>C</i> <sub>2, ref</sub>	Coefficient restore term moisture [-]	1.8
<i>a</i>	Clapp and Hornberger retention curve parameter <i>a</i> [-]	0.219
<i>b</i>	Clapp and Hornberger retention curve parameter <i>b</i> [-]	4.9
<i>p</i>	Clapp and Hornberger retention curve parameter <i>c</i> [-]	4.
Γ (298 K)	CO <sub>2</sub> compensation concentration at 298 K [mgm <sup>-3</sup> ]	4.3
<i>Q</i> <sub>10</sub> Γ	percentage of increase in Γ (298 K) with +10 K [-]	1.5
<i>g</i> <sub>m</sub> (298 K)	mesophyll conductance at 298 K [mms <sup>-1</sup> ]	17.5
<i>Q</i> <sub>10</sub> <i>g</i> <sub>m</sub>	percentage of increase in <i>g</i> <sub>m</sub> with +10 K [-]	2.0
<i>T</i> <sub>1</sub> <i>g</i> <sub>m</sub>	reference temperature <i>T</i> <sub>1</sub> for <i>g</i> <sub>m</sub> [K]	286.0
<i>T</i> <sub>2</sub> <i>g</i> <sub>m</sub>	reference temperature <i>T</i> <sub>2</sub> for <i>g</i> <sub>m</sub> [K]	309.0
<i>A</i> <sub>m, max</sub> (298 K)	CO <sub>2</sub> maximal primary productivity at 298 K [mgm <sup>-2</sup> s <sup>-1</sup> ]	1.7
<i>Q</i> <sub>10</sub> <i>A</i> <sub>m</sub>	percentage of increase in <i>A</i> <sub>m, max</sub> with +10 K [-]	2.0
<i>T</i> <sub>1</sub> <i>A</i> <sub>m</sub>	reference temperature <i>T</i> <sub>1</sub> for <i>A</i> <sub>m, max</sub> [K]	286.0
<i>T</i> <sub>2</sub> <i>A</i> <sub>m</sub>	reference temperature <i>T</i> <sub>2</sub> for <i>A</i> <sub>m, max</sub> [K]	311.0
<i>i</i> <sub>0</sub>	maximum value <i>C</i> <sub>frac</sub> [-]	0.85
<i>a</i> <sub>d</sub>	regression coefficient for <i>C</i> <sub>frac</sub> [kPa <sup>-1</sup> ]	0.15
<i>α</i> <sub>0</sub>	initial low light conditions [mgJ <sup>-1</sup> ]	0.014
<i>K</i> <sub>x</sub>	extinction coefficient for PAR [-]	0.7
<i>g</i> <sub>min</sub>	cuticular minimum conductance [ms <sup>-1</sup> ]	2.5 × 10 <sup>-4</sup>
<i>R</i> <sub>10</sub>	Respiration at 10 °C [mgCO <sub>2</sub> m <sup>-2</sup> s <sup>-1</sup> ]	0.03
<i>E</i> <sub>act0</sub>	Activation energy [kJkmol <sup>-1</sup> ]	5.33 × 10 <sup>4</sup>

**Two perspectives on coupled exchange in the boundary layer**

M. Combe et al.

[Title Page](#)

[Abstract](#)   [Introduction](#)

[Conclusions](#)   [References](#)

[Tables](#)   [Figures](#)

[⏪](#)   [⏩](#)

[◀](#)   [▶](#)

[Back](#)   [Close](#)

[Full Screen / Esc](#)

[Printer-friendly Version](#)

[Interactive Discussion](#)



**Table A3.** GECROS model initial conditions for the 4 August 2007. See Yin and van Laar (2005); Sinclair and de Wit (1975) for the rest of the maize average genotype parameters.

variable	description and unit	value
SLP	short day crop	yes
DETER	determinate crop	yes
C3C4	C4 crop	yes
LODGE	lodgingallowed	no
LEGUME	legume crop	no
NPL	plant density [plant m <sup>-2</sup> ]	9.1
EG	efficiency of germination [%]	3.6783
HTMX	maximum plant height [m]	2.8
BLD	leaf angle [deg]	50.
SEEDW	seed weight [g]	0.5
MTDV	minimal thermal days for vegetative phase [d]	41.0
MTDR	minimal thermal days for reproductive phase [d]	15.7
PSEN	photoperiod sensitivity of phenological development [h <sup>-1</sup> ]	0.
TM	development stage when transition from CB to CX is fastest [-]	1.5
CX	factor for initial N concentration of seed fill [-]	1.
CB	factor for final N concentration of seed fill [-]	1.
PNLS	fraction of dead leaf N incorporated into soil litter [-]	1.
CLAY	percentage of clay in the soil [%]	7.
WCMAX	soil water content at maximum holding capacity [m <sup>3</sup> m <sup>-3</sup> ]	0.36
WCFC	soil water content at field capacity [m <sup>3</sup> m <sup>-3</sup> ]	0.15
WCMIN	minimum soil water content [m <sup>3</sup> m <sup>-3</sup> ]	0.06
RPMRO	decomposition rate for resistant plant material [yr <sup>-1</sup> ]	0.3
DPMRO	decomposition rate for decomposable plant material [yr <sup>-1</sup> ]	10.
HUMR	decomposition rate for humidified organic matter [yr <sup>-1</sup> ]	0.02
BIOR	decomposition rate for microbial in the soil [yr <sup>-1</sup> ]	0.66
DRPM	ratio DPM / RPM of added plant material [-]	1.44
RA	residual ammonium-N in the soil [g N m <sup>-2</sup> ]	1.
FBIOC	fraction of initial microbial biomass in the soil in the initial total soil organic carbon (TOC) [-]	0.03
BHC	initial soil microbial biomass + humified soil organic matter [g C m <sup>-2</sup> ]	3500.
TOC	total organic C in the soil [g C m <sup>-2</sup> ]	7193.
RN	residual nitrate-N in the soil [g N m <sup>-2</sup> ]	1.
MULTF	multiplication factor for initial soil water status [-]	1.
TCT	time constant for soil temperature dynamics [d]	4.
RSS	soil resistance for water vapor transfer, equivalent to leaf stomatal resistance [s m <sup>-1</sup> ]	80.
SD1	thickness of upper evaporative soil layer [cm]	5.
TCP	time constant for some soil dynamic processes [d]	1.
FNA1	ammonium-N added in the 1st fertilizer application [g N m <sup>-2</sup> d <sup>-1</sup> ]	10.
FNA1T	day number at which the 1st ammonium-N dose is applied [DOY]	1.

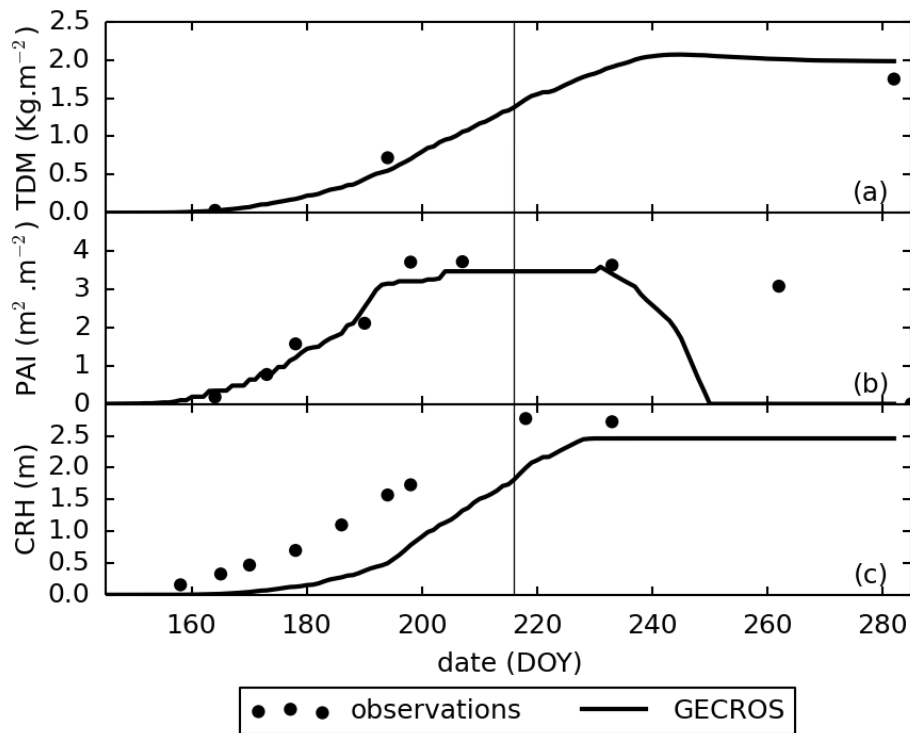


**Fig. 1.** Seasonal evolution of the **(a)** maize total dry matter (TDM), **(b)** plant area index (PAI) and **(c)** crop height (CRH), from sowing to maturity dates. The vertical continuous line represents the 4 August 2007, the date at which we dynamically couple both the MXL-GECROS and MXL-A-g<sub>s</sub> models (see assessment of these couplings in Sect. 3.2).

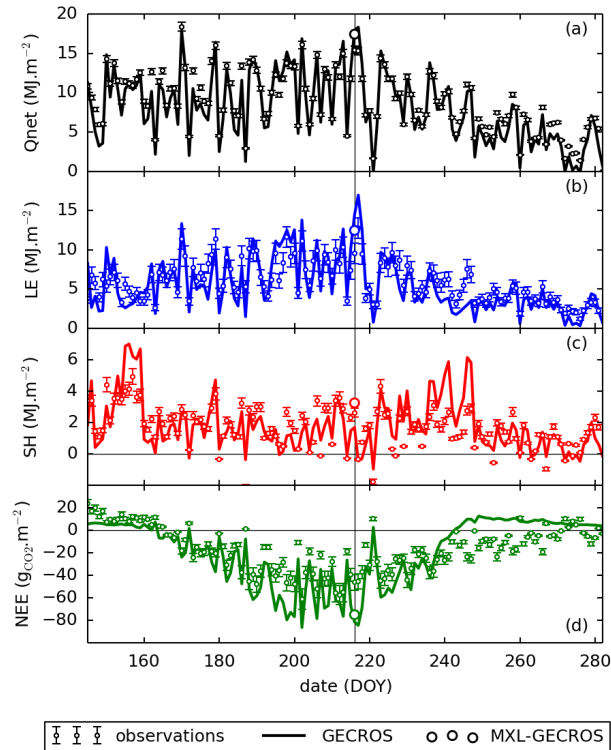


**Fig. 2.** Daily integrated **(a)** net radiation (Qnet), **(b)** latent heat flux (LE), **(c)** sensible heat flux (SH) and **(d)** net ecosystem exchange (NEE) at the maize site, from sowing to maturity dates. The integration is computed each day, using the average daytime flux times the daytime number of seconds. Days with more than 20% measurement gaps are discarded. Errors are computed as a direct sum of the Eddy Covariance random errors for instantaneous fluxes, which are presented in Sect. 4.4 of Aubinet et al. (2012). The vertical continuous line represents the 4 August 2007, the date at which we dynamically couple both the MXL-GECROS and MXL-A- $g_s$  models (see assessment of these couplings in Sect. 3.2).

Two perspectives on coupled exchange in the boundary layer

M. Combe et al.

Title Page

Abstract

Introduction

Conclusions

References

Tables

Figures

◀

▶

◀

▶

Back

Close

Full Screen / Esc

Printer-friendly Version

Interactive Discussion



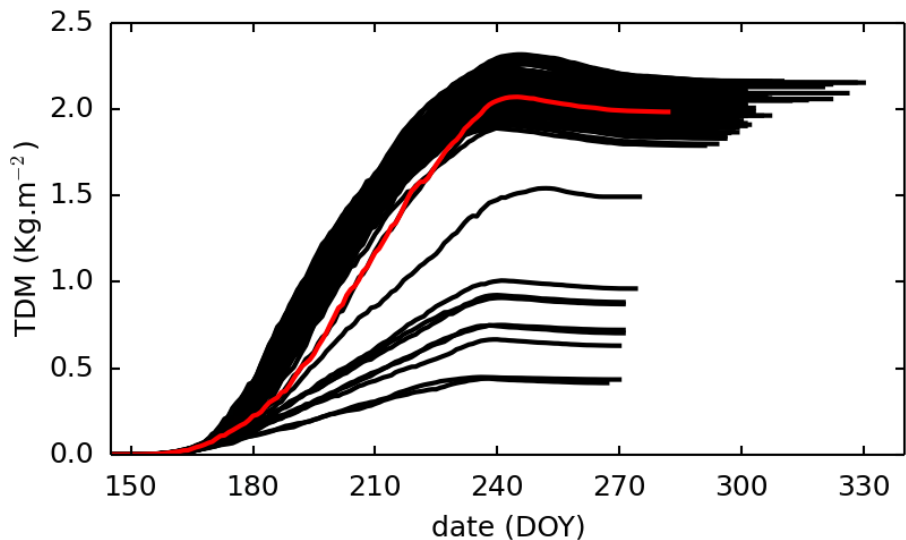


**Fig. 3.** Effect of monthly synoptic weather pattern variations on the maize total dry matter (TDM). The red curve shows the GECROS control run, from which we derived the synoptic weather variations for the other 100 runs in black (see the sensitivity analysis design in Sect. 2.4). In 9% of the cases, the model fails to grow a healthy crop.

## BGD

11, 5275–5325, 2014

### Two perspectives on coupled exchange in the boundary layer

M. Combe et al.

Title Page

Abstract

Introduction

Conclusions

References

Tables

Figures

◀

▶

◀

▶

Back

Close

Full Screen / Esc

Printer-friendly Version

Interactive Discussion



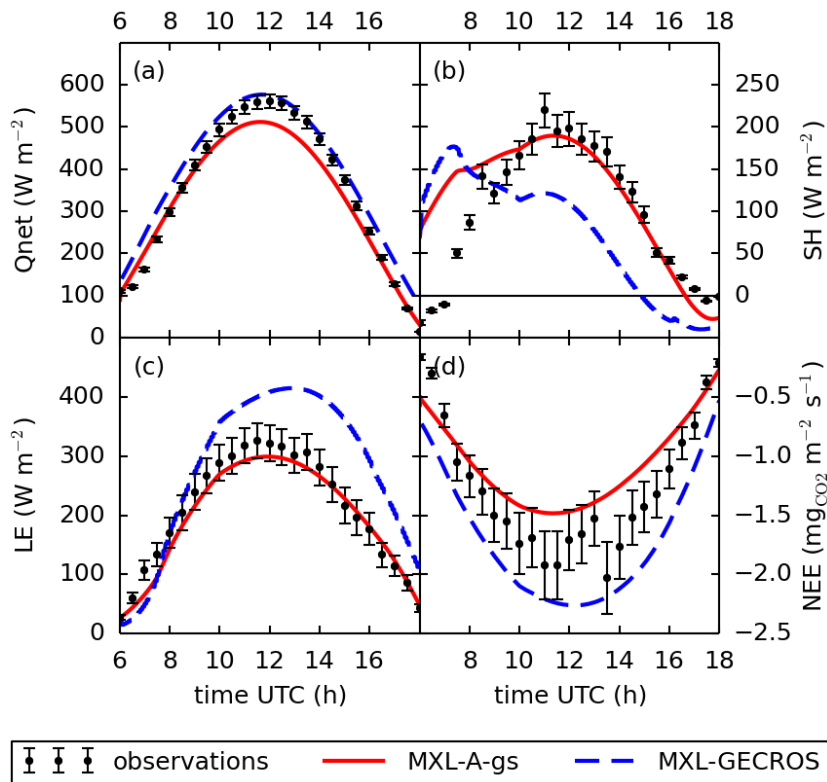


**Fig. 4.** Diurnal cycle of the **(a)** net radiation ( $Q_{\text{net}}$ ), **(b)** sensible heat flux (SH), **(c)** latent heat flux (LE), and **(d)** net ecosystem exchange (NEE), on the 4 August 2007. The error bars represent the average Eddy Covariance random errors of Aubinet et al. (2012, see Sect. 4.4). NEE is negative when  $\text{CO}_2$  is being removed from the atmosphere. Differences in NEE between the two couplings directly reflect differences in net plant photosynthesis, as soil respiration is identical between the two models.

Title Page

Abstract

Introduction

Conclusions

References

Tables

Figures

◀

▶

◀

▶

Back

Close

Full Screen / Esc

Printer-friendly Version

Interactive Discussion



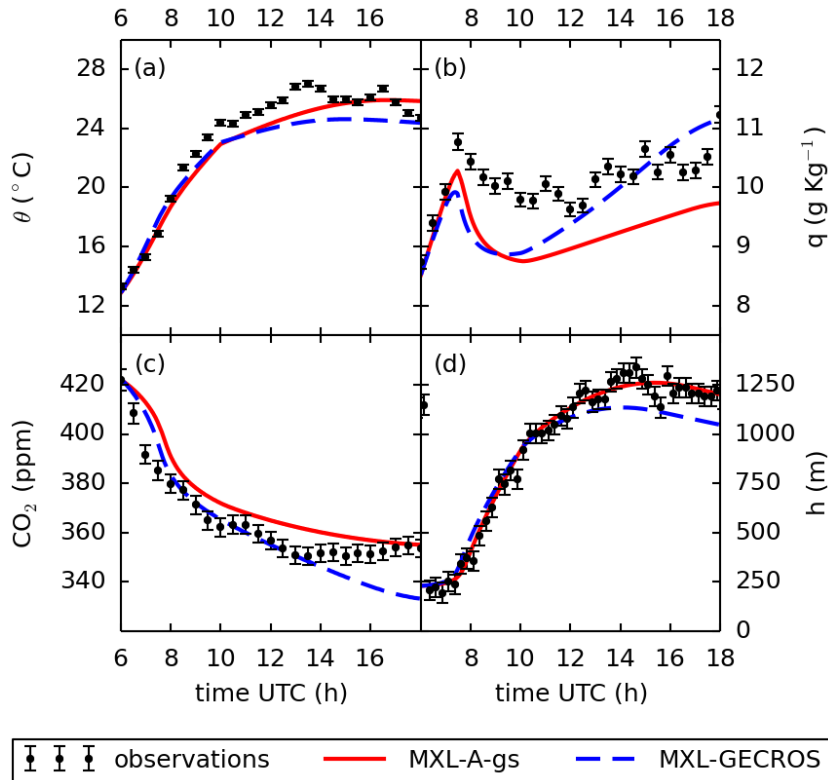


**Fig. 5.** Diurnal cycle of **(a)** the potential temperature  $\theta$ , **(b)** the specific humidity  $q$ , **(c)** the  $\text{CO}_2$  mole fraction and **(d)** the boundary-layer height  $h$ , at the maize site, on the 4 August 2007. The errors for the  $\theta$ ,  $q$  and  $\text{CO}_2$  measurements are obtained based on the factory specifications of the instruments. The error for  $h$  is assumed to be constant and equal to 50 m (personal communication, Henk Klein Baltink). Note that, in order to reproduce the early morning temperature and humidity variations, we prescribed advection of heat until 10:00 UTC and advection of humidity until 07:30 UTC (see settings in Table A1).

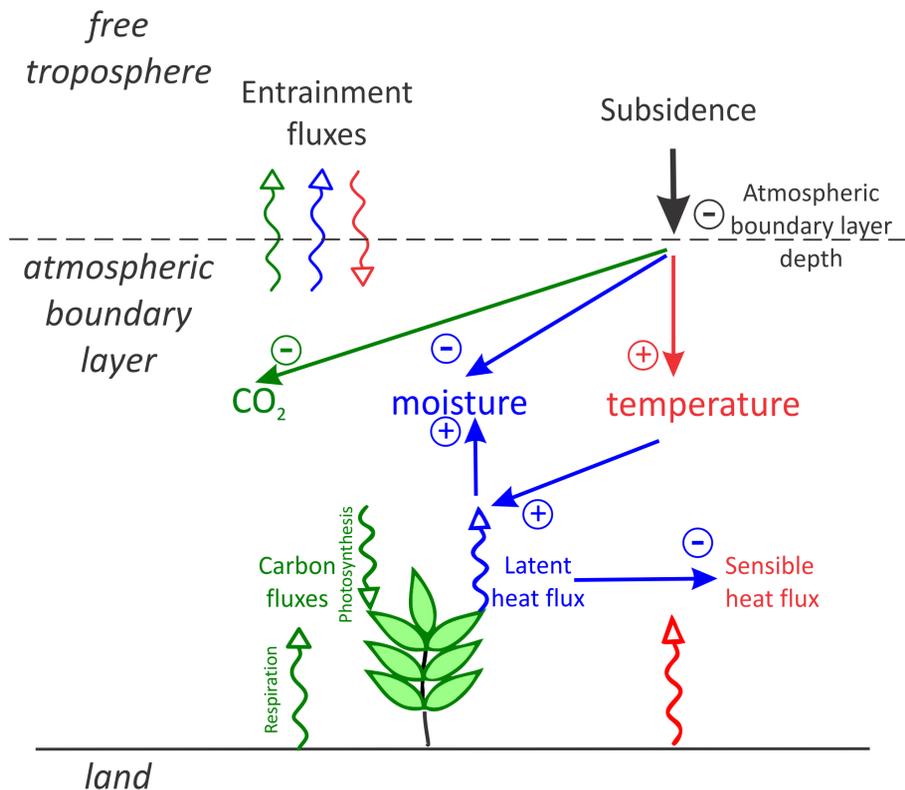


**Fig. 6.** Interactions between the carbon (green), water (blue) and heat (red) cycles in the coupled land-ABL system. Increased subsidence tends to reduce the boundary-layer height, which directly causes the ABL to warm up, dry and become CO<sub>2</sub>-depleted. This in turn affects the land-surface, which feeds back on the ABL by shifting its Bowen ratio towards more evapotranspiration.

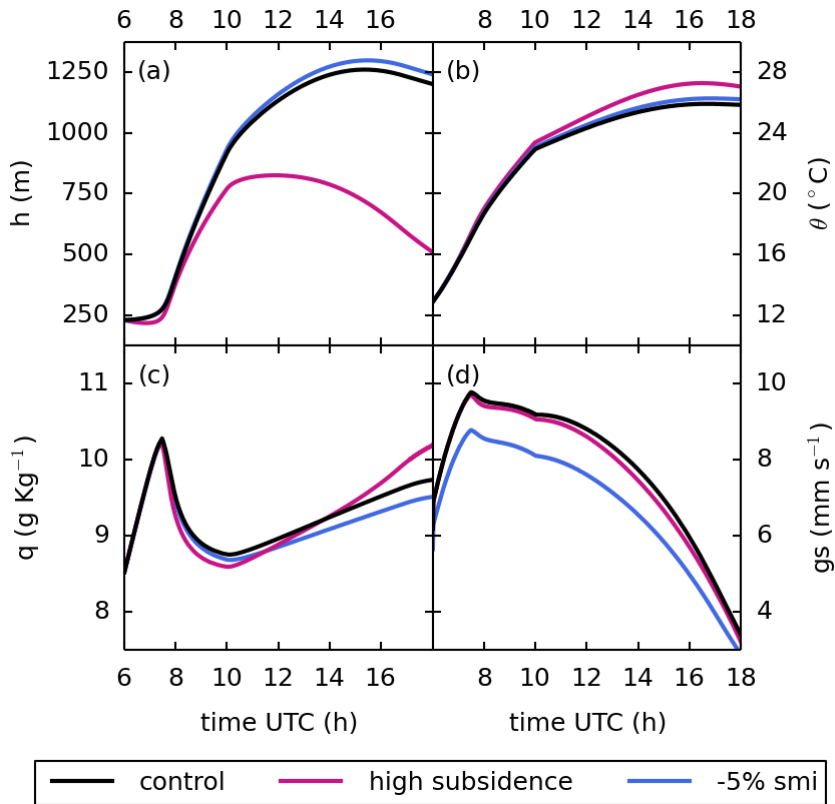


**Fig. 7.** Boundary layer and surface response to high subsidence and soil moisture depletion. High subsidence, an upper atmosphere forcing, directly impacts the boundary-layer height  $h$ , and affects the specific humidity  $q$  and the potential temperature  $\theta$ . This contrasts with soil moisture depletion, a surface forcing, which acts through the stomatal conductance  $g_s$  to impact the evapotranspiration and  $q$ .



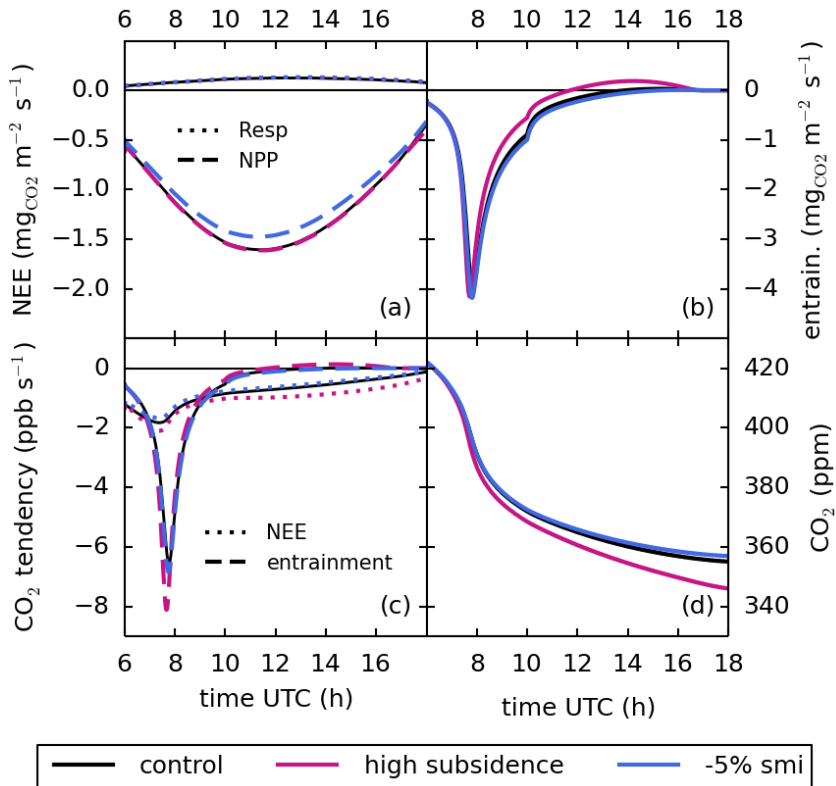


**Fig. 9.** Contributions of the surface and entrainment fluxes to the atmospheric CO<sub>2</sub> budget. Net photosynthesis (NPP) and soil respiration (Resp) combine at the surface to form NEE, while the entrainment of CO<sub>2</sub> (entrain.) takes place at top of the boundary layer. All these fluxes are negative when CO<sub>2</sub> is being removed from the boundary layer. The CO<sub>2</sub> tendencies, which determine the diurnal cycle of CO<sub>2</sub>, are obtained by dividing these CO<sub>2</sub> fluxes by the instantaneous change in boundary-layer height.